BATCH SETTLING OF SLURRIES

BATCH SETTLING OF SLURRIES

OF PRASEODYMIUM OXALATE IN WATER

By

Vuyyruru Mallareddy, B.Sc. (Tech.)

A Thesis

Submitted to the Faculty of Graduate Studies

in Partial Fulfilment of the Requirements

for the Degree

Master of Engineering

McMaster University

September 1965

Master of Engineering (1963)
(Chemical Engineering)

McMaster University
Hamilton, Ontario.

Title : Batch Settling of Slurries of Praseodymium Oxalate in Water

Author : V. Mallareddy, M.Sc.(Tech) (Andhra University)

Supervisor : Dr. E. M. Tory

Number of Pages : viii, 86

Scope and Contents:

1. A log-log plot of settling rates vs. real voidage suggests that slurries of praseodymium oxalate show three distinct types of settling: hindered, transitional and compaction.

2. The two principal variables are local solids concentration and floc structure. When the latter is constant or a function of the former, Kynch's theory holds except for the packed bed.

3. With a detector properly shielded from a radioactive slurry, the counting rate is a transform of the solids concentration. When the rate function is specified, the concentration is uniquely determined except where it is discontinuous.

4. Comparison of counting rates calculated by the application of Kynch's theory with experimental rates indicates that a concentration gradient exists in the final packed bed.

PREFACE

The work reported in this thesis may be conveniently divided into two parts. Part A deals with the settling of praseodymium oxalate slurries while Part B is concerned with the feasibility of using radioactive Pr^{142} to determine the local solids concentration in slurries.

ACKNOWLEDGEMENTS

The author wishes to thank Dr. E. M. Tory for his advice and encouragement in this work and for much of the mathematical analysis which appears in Appendix C. He also wishes to thank Dr. G. L. Keech for advice on the suitability of various isotopes and assistance in securing equipment. The contributions of Dr. D. B. Sumner and Mr. K. G. Pollock on mathematical and computational aspects of the problem are gratefully acknowledged.

TABLE OF CONTENTS

Page

TABLE OF TABLES

TABLE OF FIGURES

INTRODUCTION

In general, sedimentation, thickening, or clarification signify gravitational settling of solid particles, which are suspended in a liquid to a rather dense sludge containing a higher concentration of solids.

This unit operation is of particular interest in the field of mineral dressing, sewage treatment, de-mineralization of coal, treatment of industrial wastes, etc. Sedimentation can be carried out either in batch or continuous units.

Slurries may be either compressible or incompressible. The final solids concentration of compressible sludges increases with increasing weight of solids per unit area whereas the final concentration of incompressible sludges is not affected. Compressible sludges are generally made up of very fine particles which are grouped together in flocs. The primary flocs sometimes form aggregates which may change their shape, size or density as settling proceeds.

Types of Settling

It is customary to divide settling into categories such as "free" and "hindered". These are rough divisions depending on both the size distribution of particles and the solids concentration.

Free Settling

At very low concentrations, the particles in a polydisperse system settle individually at constant velocities which are determined primarily by particle size and density. In a system of multifarious particles, classification takes place. If the particles are very closely sized, there will be a distinct interface even at very low concentrations. In any case, the wall and other particles have an appreciable effect on the settling velocity. However, the rate of fall is of the same order of magnitude as the Stokes velocity.

Hindered Settling

Even when the particles differ greatly in size, shape and density, slurries settle with a sharp line of demarcation when the solids concentration is sufficiently high. For such slurries, the transition from "free settling" to "hindered settling" is very gradual. The first sign of the transition is the appearance of a very hazy and faint interface. This gradually becomes sharper.

In hindered settling, the particles or flocs are close together, causing the velocity gradients surrounding each particle to be greatly affected by the presence of neighbouring particles. Initially, the particles settle at constant velocity. After the constant-rate period, the velocity decreases. If this change occurs abruptly, this point is commonly called the point of compression[1].

LITERATURE SURVEY

Sedimentation of slurries and suspensions has been the subject of extensive study in the search for a comprehensive theory or empirical formula which deals with the rate of fall of a suspension over its whole concentration range. A practical application is in the design of thickners with minimum experimentation from batch settling data.

Therefore, in general, the work can be classified into

1. Batch Settling,
2. Continuous Settling.

The present work deals with batch settling of flocculent, incompressible slurries.

In their pioneer work, Coe and Clevenger[1] observed four different zones in a batch settling test with Metallurgical Slimes. Figure (1) which is reproduced from their paper gives a typical history of a suspension which is initially of uniform concentration.

Initially the column contains a uniform two-phase mixture B as shown in Figure (1a). As settling takes place, clear liquid A begins to appear at the top of the column and a dense sediment D at the bottom (Figure 1b). In between B and D, there is often a region C, in which the concentration is not uniform but varies from that of the initial concentration at BC to the maximum possible at DC. As time progresses, the depth of zones A and D increase, zone B decreases and zone C remains constant. The point at which C and D merge is called the critical point.

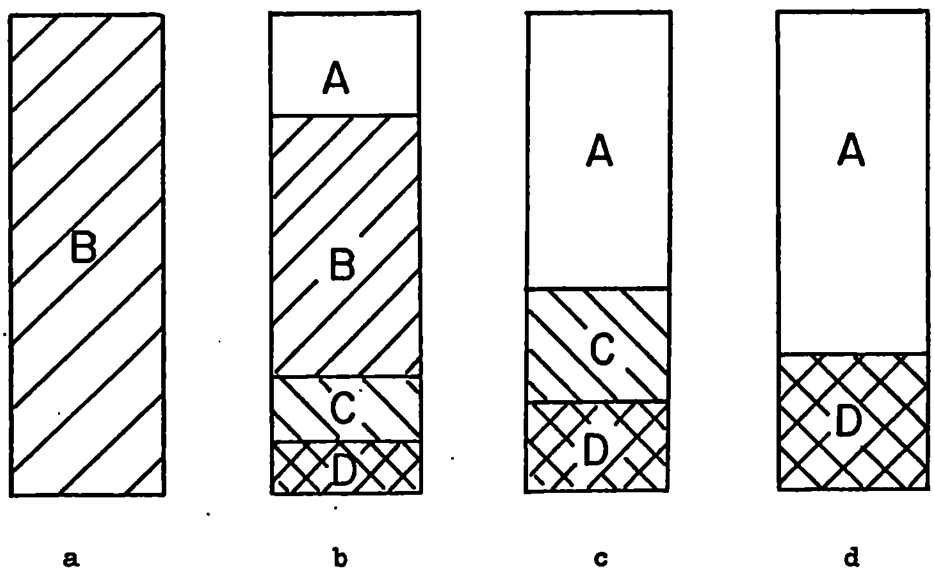

Fig. 1 History of a Typical Batch Sedimentation

Mishler[2] showed that

(a) the depth of column has no effect on the initial settling rates and the time taken for the initial slurry to settle to its final consistency is proportional to the weight of solids.

(b) at high initial concentrations, the final consistency of the sediment was greater[1], which was attributed to the sand particles present in the slurry. Deane[3] confirmed the latter observation.

Deerr[4] noticed the logarithmic appearance of settling curves after the critical point and suggested the following equation:

$$\frac{1}{t}\log\frac{Z_o - Z_\infty}{Z - Z_\infty} = k \qquad (1)$$

Robinson[5] in an attempt to correlate the velocities of suspension, modified the Stokes law and obtained the equation

$$-\frac{dZ}{dt} = k\, d^2\,(\rho_p - \rho_s)/\mu_s \qquad (2)$$

Egolf and McCabe[6] gave another version of modified Stokes Equation

$$u = \phi\, d^2\,\frac{(\rho_p - \rho_L)}{\mu_L}\;\frac{Z_o}{Z_\infty}\;(0.415 - c_\infty)^{1.4} \qquad (3)$$

for initial rates, and

$$\log\frac{Z}{Z_\infty} = K\log(Bt) \qquad (4)$$

for the compression period. It was reported that the experimentally observed values lie within ± 20% of those calculated from Equation (3).

Ward and Kammermeyer[7] pointed out that the value of c_∞ in Equation (3) is influenced by particle size and the weight concentration of the suspension. As the particle size increase c_∞ increases and may reach a value of

0.415 in which case Equation (3) is no longer valid and it is necessary to develop a new constant.

They also showed that a simple relation existed between the ratio of ultimate to initial settling heights which can be expressed as

$$\frac{Z_{\infty}}{Z_o} \; \alpha \; C_o^{\,n} \tag{5}$$

Work and Kohler[3] noticed the similarity of settling curves for the same slurry with different initial heights. From this fact, it is possible to predict the settling curve for any normal settling height, if the settling curve for any other height is established. The correlation is

$$\frac{Z}{Z_o} = f\,(k/Z_o) \tag{6}$$

However, they stated that if the slurries are not stirred, channels will form in which case deviations are expected from the similarity relationship.

Comings[9] proved experimentally that thickening is the advance upwards in succeeding waves, of higher concentrations from the bottom layers. Figure 2 of his paper clearly indicates how the concentration layers are being propagated with time. Detention time is also a variable for compressible slurries.

Kammermeyer[10], while studying the effect Z_o and C_o on final height, expressed the possibility that at high solid concentrations of the suspension or at high initial settling heights, the final height may be independent of the initial height.

Roberts[11] advanced the hypothesis "that the rate at which water is eliminated from a pulp in compression is at all times proportional to the amount which can be eliminated up to infinite time". Comings[9] results do not support this conclusion. He concludes that when the pulp is compressible and when thickening to a minimum liquid content, the depth of the compression zone is important as well as the time required for the liquid to be squeezed out of the zone.

On the same basis as Deerr[4], Roberts proposed the equation for compressible settling

$$-\frac{dZ}{dt} = k\ (Z - Z_{\infty}) \tag{6a}$$

or

$$-\frac{dD}{dt} = k\ (D - D_{\infty}) \tag{6b}$$

Richardson and Zaki[12] questioning the validity of using suspension density and suspension viscosity[5] in the modified Stokes Equation, argued that for a suspension of uniform particles, the effective buoyancy force acting on the particles is not dependent on the density of the suspension. This is true because each particle displaces its own volume of liquid as it settles, on the other hand, if a large particle is settling in a suspension of particles which are sufficiently small to behave as part of the liquid, the particles displace an equal volume of suspension.

Similarly, the effect of concentration on the resistance force encountered by a particle for a given relative velocity is attributable to the increase in the velocity gradient rather than to a change in viscosity.

By dimensional analysis they showed that

$$\frac{u}{u_o} = f\left(\varepsilon, \frac{d}{D}\right) \tag{7}$$

u = settling velocity of suspension

u_o = Stokes velocity

By extensive experimentation they showed that the sedimentation and fluidization results can be correlated[13] by a single line

log u vs. log ε

By considering the dynamic equilibrium of a suspension of uniform spherical particles settling in a fluid, Richardson and Zaki[14] obtained an expression for the settling velocity in the form of a correction factor to be used in conjunction with Stokes law.

$$u = \frac{u_o}{\beta_c} \tag{8}$$

Where β_c is a correction factor. For a suspension of uniform spherical particles

$$\beta_c = (1-c)^{-4.65} \tag{9}$$

There is much supporting evidence for the functional form of Equation (8)[13,15,16]

Michaels and Bolger[17] in their work with flocculated Kaolin suspensions assumed that the Richardson and Zaki[12] equation holds provided the flow units are flocs, and modified equation (9) to

$$u = \frac{g\, d^2(\rho_p - \rho_L)(1-\phi\, c)^{4.65}}{18\, \mu_L\, \phi} \tag{10}$$

Steinour[18] experimentally studied the sedimentation of fine-pearl tapioca particles in the laminar range and found that for porosities up to 0.8, the results could be correlated by a modified form of the Kozeny equation.

$$\frac{u}{u_o} = \frac{\varepsilon^3}{1-\varepsilon}\left\{\frac{1-\varepsilon}{\varepsilon} \exp\left[-4.19\ (1-\varepsilon)\right]\right\} \tag{11}$$

Bond[19] derived an expression for the settling velocity of suspension

$$u = u_o \quad (1-K\ c^{2/3}) \tag{12}$$

In deriving this equation, he assumed that the relative velocity between the slurry and the fluid always remains constant and is equal to the Stokes velocity of the particles. This cannot be true, because the relative velocity is a function of the concentration of solids and is given by

$$u_R = \frac{u}{1-c} \tag{13}$$

Kynch[20] was apparently the first to formulate a comprehensive mathematical theory of sedimentation on the sole assumption that the velocity of fall is a function of the local solids concentration. Using a plot of total solids flow rate against concentration he was able to derive the velocity of surfaces of discontinuity and to predict that particular values of concentration would be propagated through the sediment with particular characteristic velocities. From continuity relationships the local solids concentration can be calculated from

$$c = \frac{C_o Z_o}{Z+ut} \tag{14}$$

It was shown that if any discontinuity exists, it will be propagated upwards with a velocity given by

$$\delta = \frac{S_1 - S_2}{c_2 - c_1} \tag{15}$$

If the change in particle concentrations is small, the expression for δ reduces to

$$\delta = -\frac{dS}{dc} \tag{16}$$

Once the S vs. c curve is established, the possible modes of settling curves can be established. Using equation (14) the S vs. c curve can be established from one batch settling test.

Work and Kohler's[8] calculations support Kynch's theory. The most striking resemblance to Kynch's theory is their calculations of average concentration at equal slopes from various settling curves of different initial concentrations and equal initial height. From similar triangles, their results can be used to calculate surface concentrations. Mishler's[2] results are those expected on the basis of Kynch's theory.

Yoshika et al[21] found that the constant K in equation 6a and 6b varies inversely with C_oZ_o. In the modified form Roberts[11] equation is written as

$$-\frac{dZ}{dt} = \frac{K'}{C_oZ_o}(Z - Z_\infty) \tag{17}$$

where K' is a true constant for any given material. They gave experimental support to Kynch's[20] theory and developed a relationship between final reduced height and weight of solids per unit area

$$\frac{Z_\infty}{C_oZ_o} \alpha \ (C_oZ_o)^{-n} \tag{18}$$

This equation is of the same type as equation (5). Smellie and Lamer[22] studied the sedimentation of flocculated suspensions and gave an empirical equation

$$K/(Z_o - Z) = \alpha + \beta t \tag{19}$$

They erroneously derived this equation from the continuity equation of Kynch[20]. Errors in their mathematical analysis led them to assume that the volume concentration of solids is at any instant uniform through out the settling column, which is quite contrary to the idea of concentration gradients.

Shannon and Tory and associates[23, 24, 25] developed a method for calculating complete settling curves from initial rates and verified Kynch's theory for slurries of closely sized spheres in water.

Tory[26] has shown that equations 14 and 17 could be combined to get equation 20 from which concentration vs. velocity can be calculated without recourse to the sedimentation curve.

$$\frac{1}{C} = \frac{1}{C_\infty} + \frac{u}{u_o}\left(\frac{1}{C_e} - \frac{1}{C_\infty}\right) + \frac{u}{k'} \ln \frac{u_e}{u} \qquad (20)$$

This equation is more convenient than using tangents to the settling curve, where settling is slow. He has also shown that equation 18 holds good for several results in the literature including some which had been attributed to the effect of initial concentration. He also noted the importance of concentration gradients for settling rates of $CaCo_3$ slurries. Additional support for Kynch's theory is given by Hascott[27], Wallis[28], Boyd and Whitton[29].

EXPERIMENTAL

Materials

Praseodymium oxalate, $Pr_2(C_2O_4)_3 \cdot x\,H_2O$, (Code 719.9, Lindsay Chemical Division of American Potash and Chemical Corporation) was used as a finely divided solid for settling studies.

In order to establish the effect of aging on its settling properties, settling rates were determined as a function of age. From Figure 2, it appears that the settling properties change slightly with agitation. A thick master slurry was made and stirred vigorously for more than a week. The particle size distribution of a small sample of this slurry can be estimated from Figure 3.

All samples for settling tests were taken from this master slurry. Both the weight and volume of slurry were measured and the weight of solids was calculated. The apparent density of praseodymium oxalate was determined experimentally to be 2.522 ± 0.0075 g./cc.

Procedure

The same slurry sample was used for a series of runs, the solids concentration in the cylinder being adjusted by adding or removing water. The slurry was mixed thoroughly with a perforated stainless steel plunger until the solids apparently were distributed uniformly throughout the slurry.

The time was counted from the moment the plunger was taken out of the slurry. The level of the interface as a function of time was recorded. (If the level falls very rapidly for just a very short time, the slurry

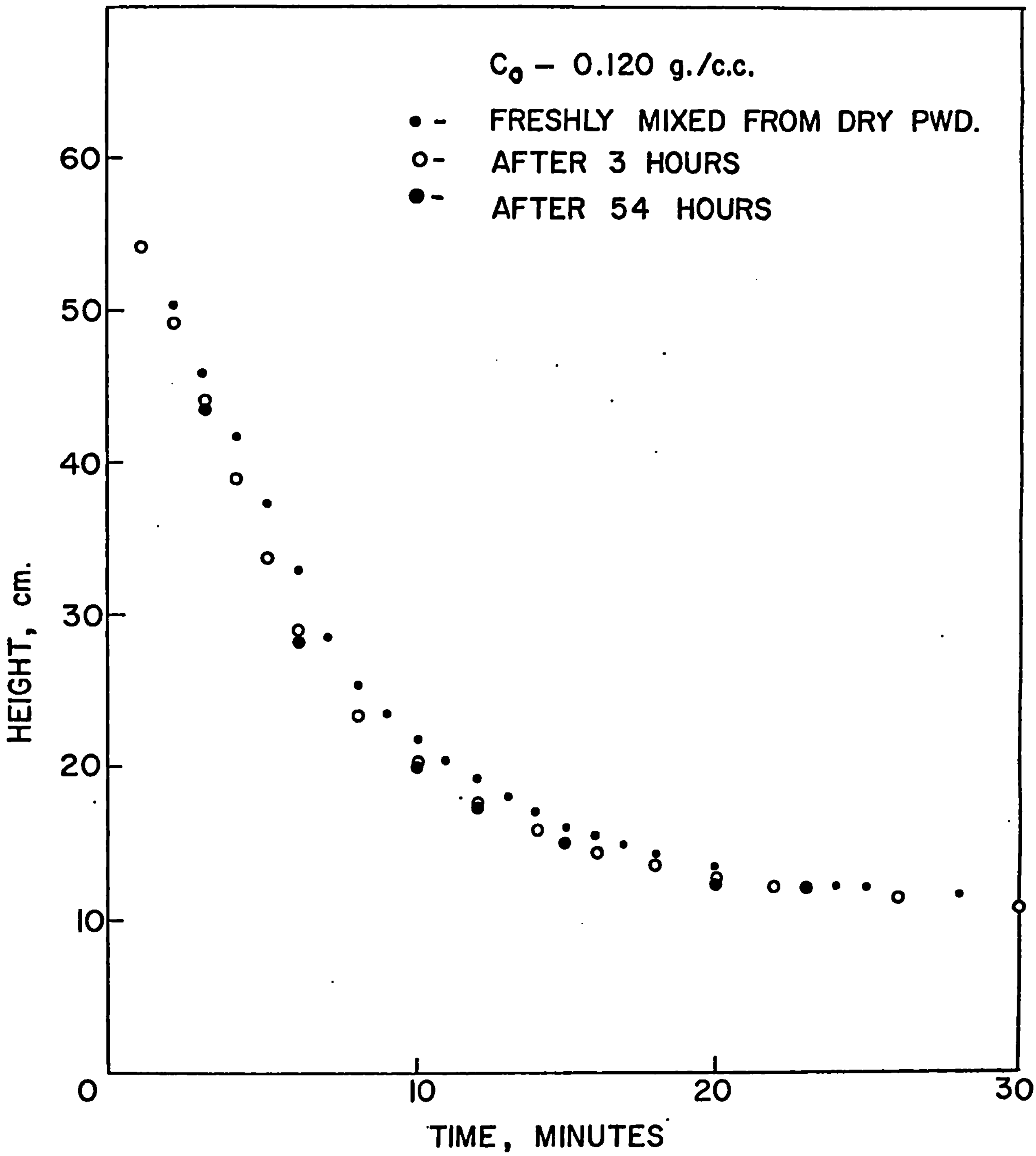

Fig. 2 Effect of Aging on Settling Properties

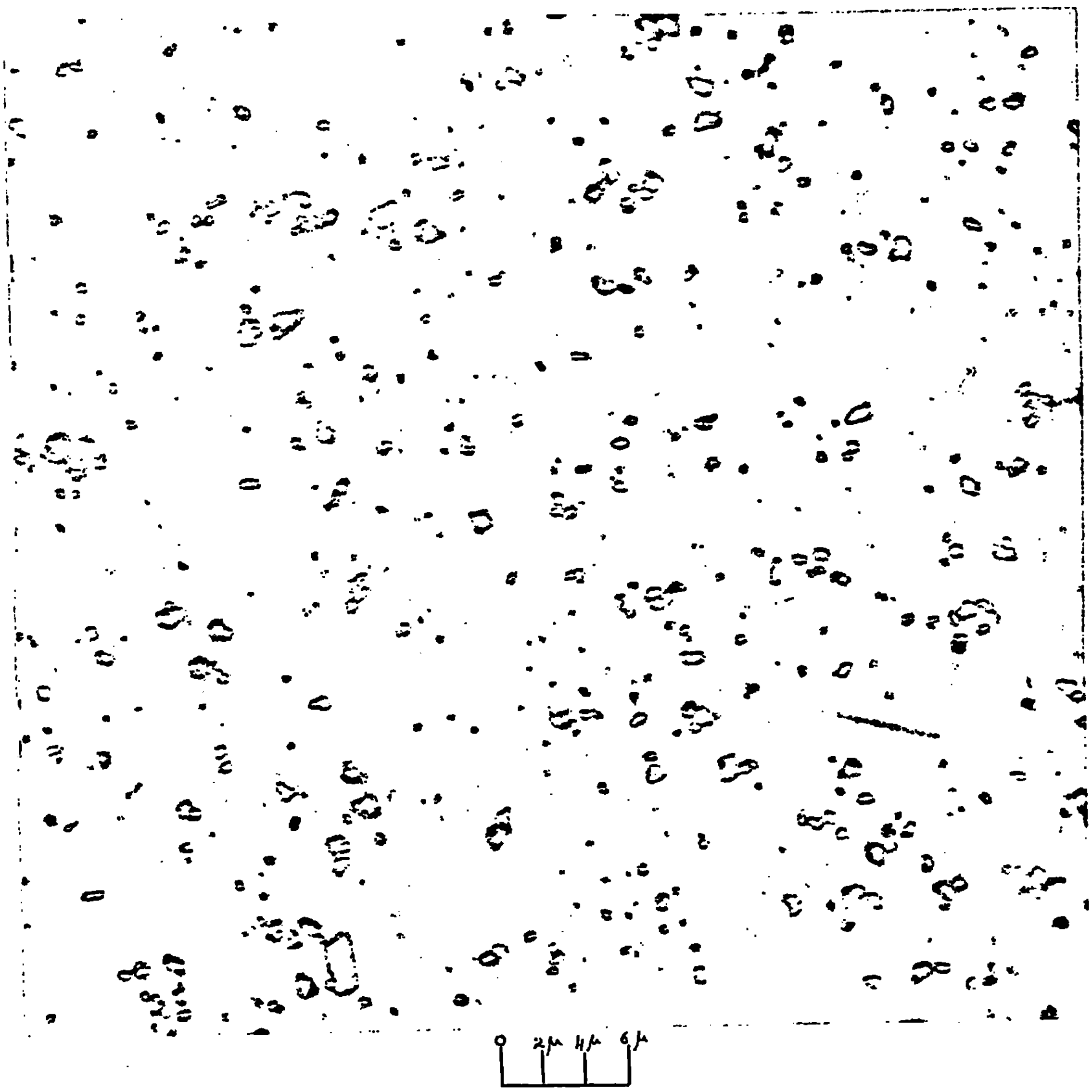

Figure 3. Photo micrograph of Praseodymium Oxalate Particles

is not uniform, i.e. the solids concentration near the interface is lower than in the bulk of the slurry). The frequency of readings varied from four per minute to one per five minutes depending on the velocity of fall. A series of tests was done in which each solids concentration was run twice for each batch. The order of runs was determined by lot.

The technique which gave the most reproducible results was as follows. First, 280g. of solids were added to the column and settling tests were carried out. A known weight of solids was removed from the column and settling tests were repeated. This was continued until the data covered a wide range of concentrations. A cathetometer was used to reduce the observational error in runs involving the slow compaction of thick slurries.

The large ratio of length (90.0 cm) to diameter (4.65 cm I.D.) of the column made it possible to study a wide variety of concentrations with relatively little material. However, the diameter was large enough to ensure that wall effects would be negligible for discrete particles or flocs.

RESULTS

Initial Settling Rates

Initial settling rates were obtained for a wide range of initial concentrations and several weights of solids. The most reproducible results are shown in Tables 1, 2 and 3, the remainder are given in Appendix A. From the relatively fast settling rates for all concentrations, it is obvious that the solids do not settle as individual particles. It appears that the basic units are small clusters of particles with enclosed liquid which are called flocs. These flocs have a certain amount of mechanical strength and so are able to retain their identity under the very mild surface shear forces and collisions experienced in gravity settling.

To establish the functional relationship between velocity and concentration, the logarithm of the initial constant rate was plotted against the logarithm of void fraction. Figure 4 shows that there are three definite regions. Corresponding to these three functional relationships, three types of settling may be postulated: hindered settling, transitional settling and compaction.

Hindered Settling

The lowest concentration used was the minimum needed to obtain a distinguishable interface between the sediment and the supernate. At low concentrations, many particles are left behind; the supernate is white with small particles which settle very slowly. These are individual particles which were too far from any floc to be taken up.

TABLE I

Batch 7

Initial Settling Rates vs. Initial Concentrations.

Weight of Solids 280.4 g.   Temperature 26-27°C.

Height z_o (cm)	Concentration C_o (g./cc)	Void fraction ε	Rate of settling u (cm/min)
26.10	0.6325	0.7492	0.02155
27.10	0.6092	0.7585	0.02577
27.50	0.6003	0.7620	0.02693
29.00	0.5683	0.7747	0.03041
30.00	0.5500	0.7818	0.03661
31.50	0.5240	0.7922	0.04246
33.30	0.4957	0.8035	0.05205
34.80	0.4737	0.8122	0.0606
36.10	0.4567	0.8190	0.06482
37.50	0.4400	0.8255	0.06858
38.10	0.4333	0.8282	0.1904
39.60	0.4168	0.8347	0.080
41.00	0.4026	0.8404	0.09539
42.65	0.3870	0.8465	0.1052
42.65	0.3870	0.8465	0.2265
45.85	0.360	0.8573	0.2536
49.75	0.3318	0.8685	0.2778
55.00	0.300	0.8810	0.3072

Height z_o (cm)	Concentration C_o (g./cc)	Void fraction ε	Rate of settling u (cm/min)
62.50	0.2641	0.8953	0.3860
75.00	0.220	0.9127	0.5283
80.00	0.2063	0.9182	0.6083
85.00	0.1942	0.9230	0.6370
90.00	0.1834	0.9273	0.7558

TABLE 2

Batch 8

Initial Settling Rates vs. Initial Concentrations.

Weight of Solids 213.6 g. Temperature 26-27°C.

Height z_o (cm)	Concentration C_o (g./cc)	Void fraction	Rate of settling u (cm/min)
25.0	0.5030	0.8006	0.04838
27.0	0.4657	0.8154	0.06154
30.0	0.4191	0.8353	0.2353
40.1	0.3136	0.8757	0.2777
45.0	0.2794	0.8892	0.3334
50.0	0.2515	0.9003	0.4166
55.0	0.2286	0.9094	0.50
60.0	0.2095	0.9169	0.5983
65.0	0.1934	0.9233	0.6818
70.0	0.1796	0.9288	0.7843
75.0	0.1676	0.9334	0.9230
80.0	0.1572	0.9375	1.0939
85.0	0.1479	0.9414	1.2937
90.0	0.1397	0.9446	1.[illegible]129
95.0	0.1[illegible]23	0.9476	2.0280

TABLE 3

Batch 9

Initial Settling Rates vs. Initial Concentrations

Weight of Solids 155.0 g.   Temperature 26–28°C

Height Z_o (cm)	Concentration C_o (g./cc)	Void fraction	Rate of settling U (cm/min)
18.0	0.5069	0.7[illegible]8	0.04575
20.0	0.4563	0.8191	0.06436
25.0	0.3650	0.8553	0.2285
30.0	0.3042	0.8794	0.2930
35.0	0.2607	0.8966	0.3560
43.5	0.2097	0.9168	0.5983
50.0	0.1825	0.9276	0.7595
55.0	0.1659	0.9342	0.9160
60.0	0.1520	0.9397	1.1764
65.0	0.1404	0.9444	1.5304
70.0	0.1303	0.9483	1.8907
75.0	0.1216	0.9518	2.2516
80.0	0.1140	0.9548	2.702
85.0	0.1073	0.9575	3.0612
90.0	0.1014	0.9598	3.4483

A long initiation period was noted, especially at low concentrations. The more dilute the slurry, the longer this period. The long initiation period at low concentrations reflects the difficulty in forming flocs when particles are widely separated. The floc size or the number of flocs reaches an equilibrium condition, at which state, the rate of fall becomes constant. The most probable shape of floc is a sphere since this is the most stable configuration. It has been shown by Reich and Vold[30] that flocs tend to approach a uniform size in any shear field.

With low concentrations and low initial heights, steady rates are not attained because the solids concentration at the interface increases before the initiation period is complete. Therefore, initial velocities determined for concentrations less than 0.1 g./cc with initial heights of less than 80 cm are not accurate. Longer colums are needed, but in this case the mixing is not efficient enough to produce a uniform initial concentration.

Results for the hindered settling region are fitted by the equation

$$u = 25.49\ \varepsilon^{48.84} \tag{21}$$

which is a straight line on a log-log plot (Figure 4). The data shown are for batch numbers 7, 8, 9. The effect of flocculation was to increase the value of the exponent, n. For batches 1, 2, 3, and 4, it varied from 38.7 to 41.5. If n is a measure of the degree of flocculation, then the amount of flocculation increases as the age of the slurry increases.

The strongest dependence on voidage, i.e.,the largest value of n, should occur when the flocs are loose and bulky. A change in floc structure is then indicated by a change in the slope of the curve in Figure 4. Thus, a change occurs at the division between hindered settling and

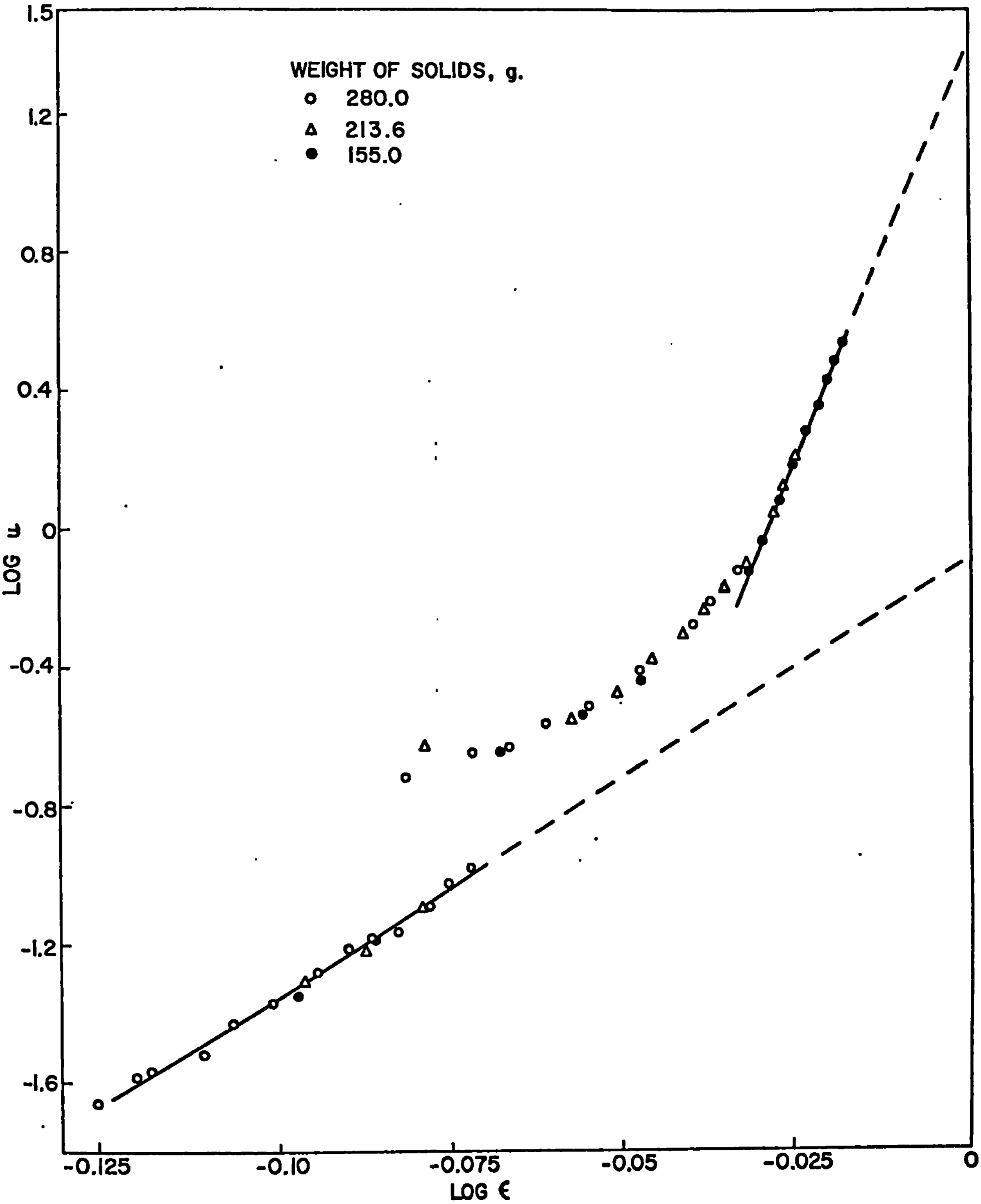

FIG. 4 LOG u vs. LOG ϵ

transitional settling, but it is difficult to know whether this change is abrupt or gradual.

In any case, if it is assumed that the change occurs because the flocs are close together, it is possible to estimate roughly the ratio of floc volume to its solid content. Assuming that the flocs are spherical and are arranged in a regular cubic array, the volume fraction of flocs, when they are fully packed, is 0.524. This occurs at a volume fraction of 0.0667. If all the praseodymium oxalate is in floc form, the ratio of floc volume to solid volume is 0.524/0.0667 = 7.86. For random packing it would be 0.610/0.0667 = 9.15. It is by no means necessary that the flocs touch each other before their volume begins to decrease. Hence, the ratio may be considerably less.

Transitional Settling

A significant feature of the division between hindered and transitional settling is that the curve (Figure 4) is continuous, although its derivative may not be. The kind of critical point, or point of compression, postulated by Coe and Clevenger presupposes a discontinuity in settling rate. In the present case, although the flocs may be close together, the water is not "squeezed" out of them.

It appears that there is a modification of the flow patterns around the flocs. Initial settling rates are very low but increase with time. From the beginning of settling, the bed develops cracks; these grow into channels through which liquid flow can be observed. This is followed by spout formation at the interface which makes it difficult to read the interface level correctly. Channel formation is abrupt, and the rate of settling increases suddenly to a new value. The time taken for channel formation decreases progressively as the concentration increases. Visually, the slurry appears to be a network, but it is uncertain whether this is real or not.

As the initial concentration is increased, the settling velocity decreases abruptly; there is a discontinuity in the velocity-voidage curve. As shown in Figure 4, there is a range of concentrations for which the rate can have either of two values. In Figure 4, the transitional region begins at a void fraction of 0.934 and ends around 0.834. This range varies from batch to batch and from run to run.

The final concentration is the same, within experimental error for all initial concentrations in the hindered and transitional regions.

Compaction

As the solids concentration is further increased, the bed settles very evenly and no channels are formed. The rate of fall is constant until almost the end. For highly concentrated slurries, the surface is curved. Apparently the walls help to support the slurry[17]. (With tubes of larger diameter, the curvature will be minimized and more precise data can be taken).

Initial settling rates are correlated by

$$u = 0.810\ \epsilon^{12.6} \qquad (21a)$$

The smaller values of the "Stokes velocity" and the exponent indicate a smaller, more compact floc than in hindered settling. Additional evidence for this view is the fact that the final solids concentration is always greater than can be obtained in either hindered or transitional settling.

In compaction, the final sediment volume is a function of initial concentration; the final concentration increases with increasing initial concentration. This seems to indicate more compact flocs. Tapping the container resulted in a higher final concentration, presumably by packing the same flocs more closely.

TABLE 4

Batch 8

Effect of Initial Concentration on Final Concentration in Compact Settling

Weight of Solids 213.6 g.

Height Z_o (cm)	Initial Concentration C_o g./cc)	Final Height Z_∞ (cm)	Final average Concentration C_∞ g/cc
19.2	0.6550	18.05	0.6967
20.0	0.6283	18.20	0.6909
21.20	0.5932	18.40	0.6835
22.1	0.5690	18.70	0.6725
23.25	0.5410	18.70	0.6725
24.20	0.5196	19.00	0.6618
25.20	0.4990	19.35	0.6500
26.30	0.4782	19.30	0.6515
28.10	0.4475	19.40	0.6482
30.00	0.4192	19.30	0.6515
31.5	0.3992	19.30	0.6515

APPLICATION OF KYNCH THEORY

Kynch's[20] theory was derived on the assumption that the rate of fall is a function of local solids concentration and the particle does not change its shape and size, i.e. the total number of particles is the same at all times. It is also applicable if floc size and structure are dependent only on the local solids concentration. Using a plot of total solids flux against concentration, he was able to derive the volicity of surfaces of discontinuity and to predict that particular values of concentration would be propagated through the sediment with particular characteristic velocities. Once the flux plot is determined, it is possible to draw all the settling curves for that particular form of flux plot.

Construction of Flux Plot

From the initial rate data, of Tables 1, 2 and 3, a flux plot was constructed (Figure 5). The dotted line indicates extrapolated values.

In the dilute region, Equation (21) was used to extrapolate. The validity of this extrapolation is doubtful at very dilute concentrations, because the floc structure varies and Equation (21) is no longer valid.

At high concentrations, the settling column was tapped until the solid no longer settled, and this was taken to be the fully packed bed at which the solids flux is zero.

Kynch[20], Tory[26], and Wallis[28] have shown how different modes of settling curves can be expected from the shape of flux plot.

Settling Curves derived from Flux Plot

In the literature many types of hypothetical flux plots have been

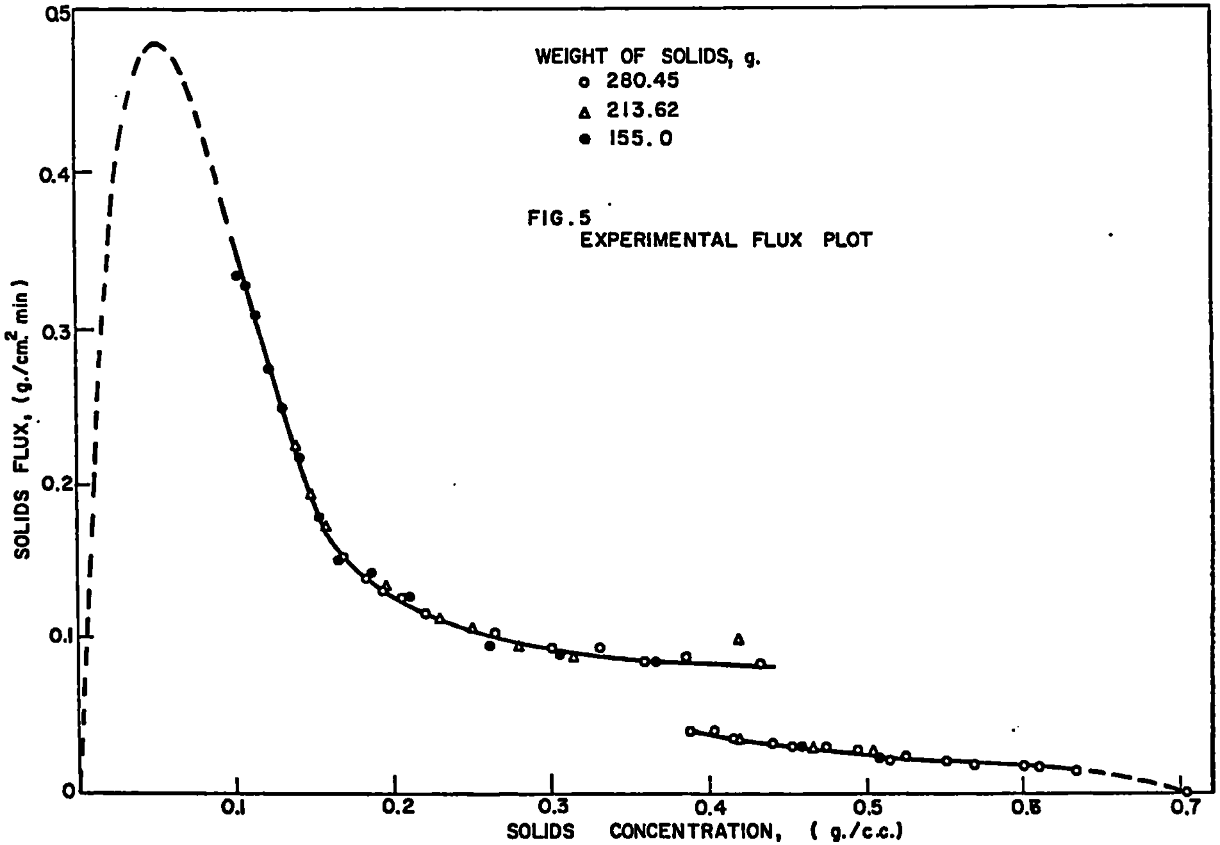
WEIGHT OF SOLIDS, g.
o 280.45
Δ 213.62
● 155.0
FIG. 5
EXPERIMENTAL FLUX PLOT
SOLIDS FLUX, (g./cm.² min)
0
0.1
0.2
0.3
0.4
0.5
0.1
0.2
0.3
0.4
0.5
0.6
0.7
SOLIDS CONCENTRATION, (g./c.c.)

assumed, which are continuous, starting from the simplest curve which is everywhere concave downwards, and with one or two inflection points introduced in the curve, but no break in the flux plot. The present flux plot shows one inflection point at a concentration of .101 g/cc and a break, which cannot be determined exactly. A similar type of curve was reported for $CaCO_3$ (Tory[26]) although it is uncertain whether his curve was continuous or discontinuous. As it is impossible to draw the theoretical settling curve without assuming the position of the break, it was assumed that the break occurs at a concentration of 0.42 g/cc.

Determination of Settling Curves from Flux Plot

Since experimental data are not available for concentrations less than 0.092, this value was chosen as the one affording comparison with experimental values over a maximum range of local solids concentrations.

The settling velocity of the interface is obtained from the flux plot by measuring the slope of the chord joining C=0 to C=C, which is equivalent to S/C. The position of the concentration gradient (continuity wave) at any time is given by $Z = \delta t$. The propagation velocity is also given by the derivative of the flux with respect to concentration. Since u and δ are both functions of concentration only, for a given suspension they may be regarded as functions of each other. The slope of the falling rate period of a sedimentation curve therefore always has a particular slope u when it crosses a line of slope δ from the origin. Therefore, all curves for various initial heights and concentrations have the same shape. This can be true only if the propagation velocity of any concentration layer is not affected by the concentration gradients which are developed in the settling column.

Thus once the flux plot is determined, all the family of settling curves can be established. Assuming that the propagation velocity is not affected by the concentration gradients, Figure 6 is determined from the flux plot.

Experimental curves for hindered and transient settling are given in Figures 7 and 8. They do not agree with settling curves derived from the complete theoretical flux plot (Figure 6) but are consistent with those deduced from that portion based on initial rates in hindered and transient settling. The large loose flocs in hindered and transitional settling cannot follow the flux plot for the small dense flocs in compaction; neither can they reach the maximum compaction acheived by the denser flocs.

The initial part (first 12 minutes) of the experimental curves shown in Figure 7, is consistent with the flux plot. Kynch's theory predicts that all results for hindered settling will merge in a common line; this is exactly the case experimentally, but the line is not that predicted from the complete flux plot.

For the curves shown in Figure 8, the maximum solids concentration was 0.612 g./cc. If this point is joined to the part of the flux plot pertaining to hindered and transitional settling, the resulting flux plot predicts the experimental curves very closely. For initial concentrations less than 0.264 g./cc, the theoretical settling curve is initially a straight line. Then follows a gradual decrease in rate and finally a sharp break in the curve as the final concentration is reached. Theoretically, this break occurs at the same point for all initial concentrations between 0.008 and 0.264 g./cc. For initial concentrations

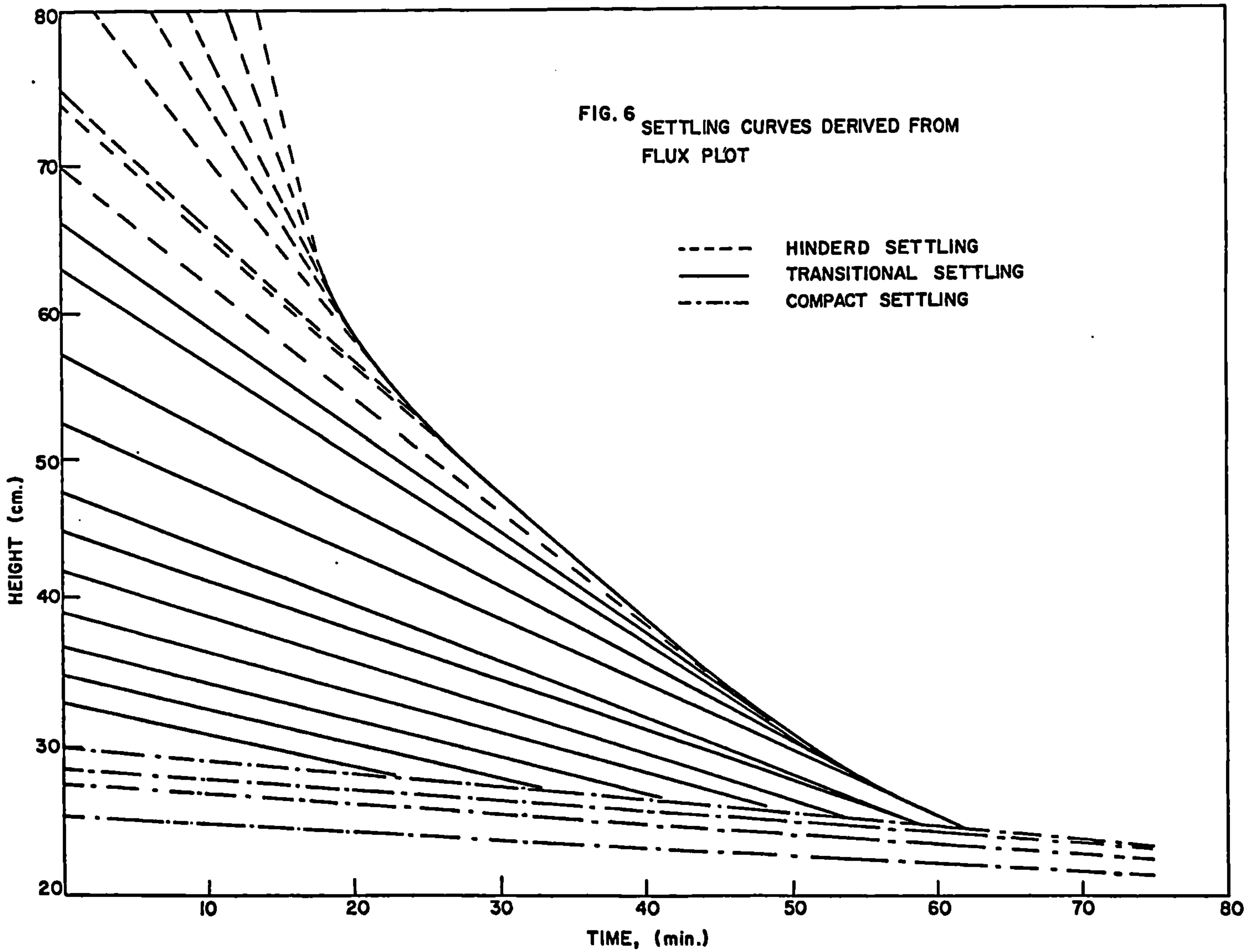
FIG. 6 SETTLING CURVES DERIVED FROM FLUX PLOT
HINDERD SETTLING
TRANSITIONAL SETTLING
COMPACT SETTLING
HEIGHT (cm.)
TIME, (min.)
80
70
60
50
40
30
20
10
20
30
40
50
60
70
80

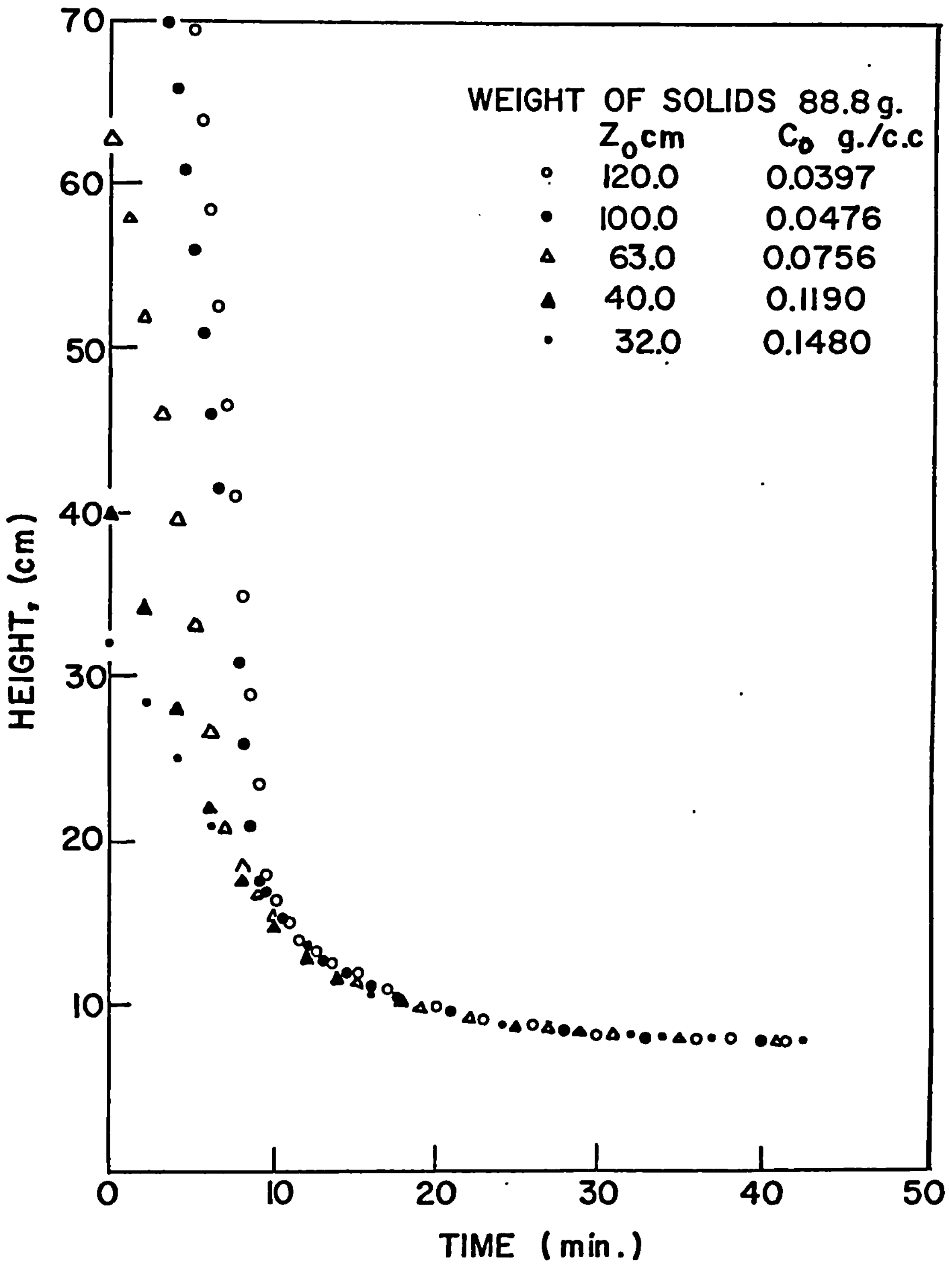

Fig. 7 Experimental Hindered Settling Curves.

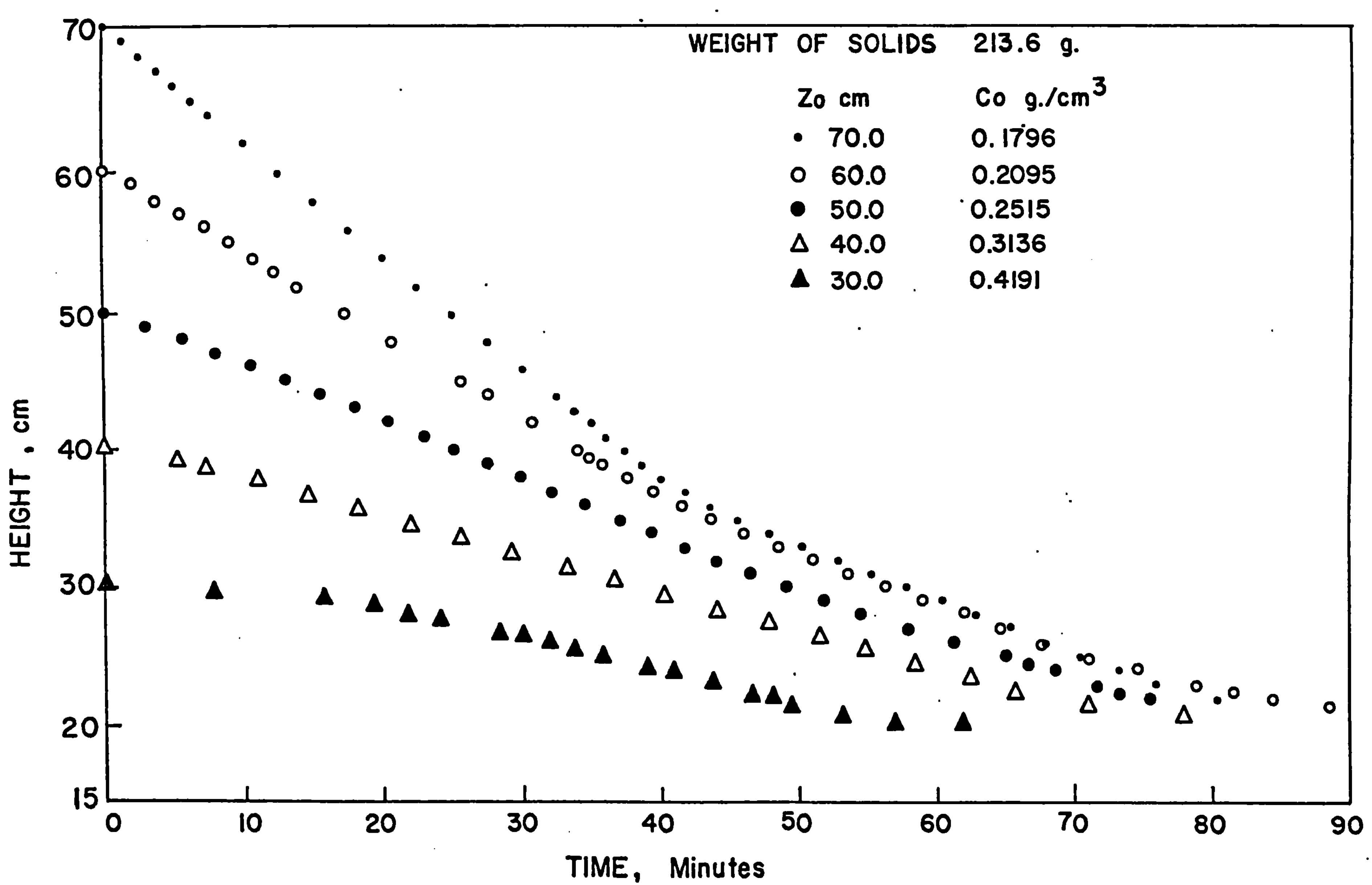

Fig. 8 Experimental Transitional Settling Curves.

greater than 0.264, the total time decreases as the concentration increases. This is in accord with the experimental results of Figure 8. The region from 0.36 to 0.44 g/cc is very unstable. Settling rates may be high from the beginning or they may be initially low and increase to a high rate. In the latter case the high value is the one used for the flux plot, the low value being considered as part of an initiation period. This is common practice[31] but should be borne in mind in assessing the agreement between theoretical and experimental curves. Instead of coming abruptly to an end, the experimental curves for transitional settling have a short period of very slow settling after the sharp break.

In compaction, the experimental results agree with the theoretical if the final solids concentration corresponds to that obtainable with the particular initial concentration.

Having shown how the flux plot can be utilized in constructing the settling curves, it was necessary to test whether the flux varies with the weight of solids, that is, whether the solids are compressible or not. This effect can be shown by plotting various settling curves of the same concentration with different initial heights and noting whether the curves are similar as was done by Work and Kohler[18]. This was shown in Figure 9 for four different initial heights and an initial concentration of 0.14 g./cc. Line a radiating from the origin separates the constant and the falling rate periods. The other radiating lines are drawn at random, from the origin. The distances AB, AC etc. are measured. When the ratios of AB to AC etc. were calculated, it was found that for a given pair of curves these ratios were equal to one another and were also equal to the ratios of the initial heights of the column.

The maximum deviation is about 4%. This deviation can be expected, because of the channel formation in the column. Having shown the validity of the geometric similarity, it is possible to generalize the settling curve by plotting Z/CoZo vs. t/CoZo as was done by Yoshioka et al[21]. If the reduced height is plotted against reduced time for various concentrations and heights, a single curve in the falling rate period, and straight lines of various slopes in the constant rate period should be obtained, if the weight of substance has no effect on the settling rate. The results are shown in Figure 10 for one initial concentration and four different weights of solids. This result is exactly that expected from Kynch's theory. The factor $\frac{1}{C_o Z_o}$ induces all the points of equal slope to coincide at one point. It was shown by Wallis[20] that the flux plot and

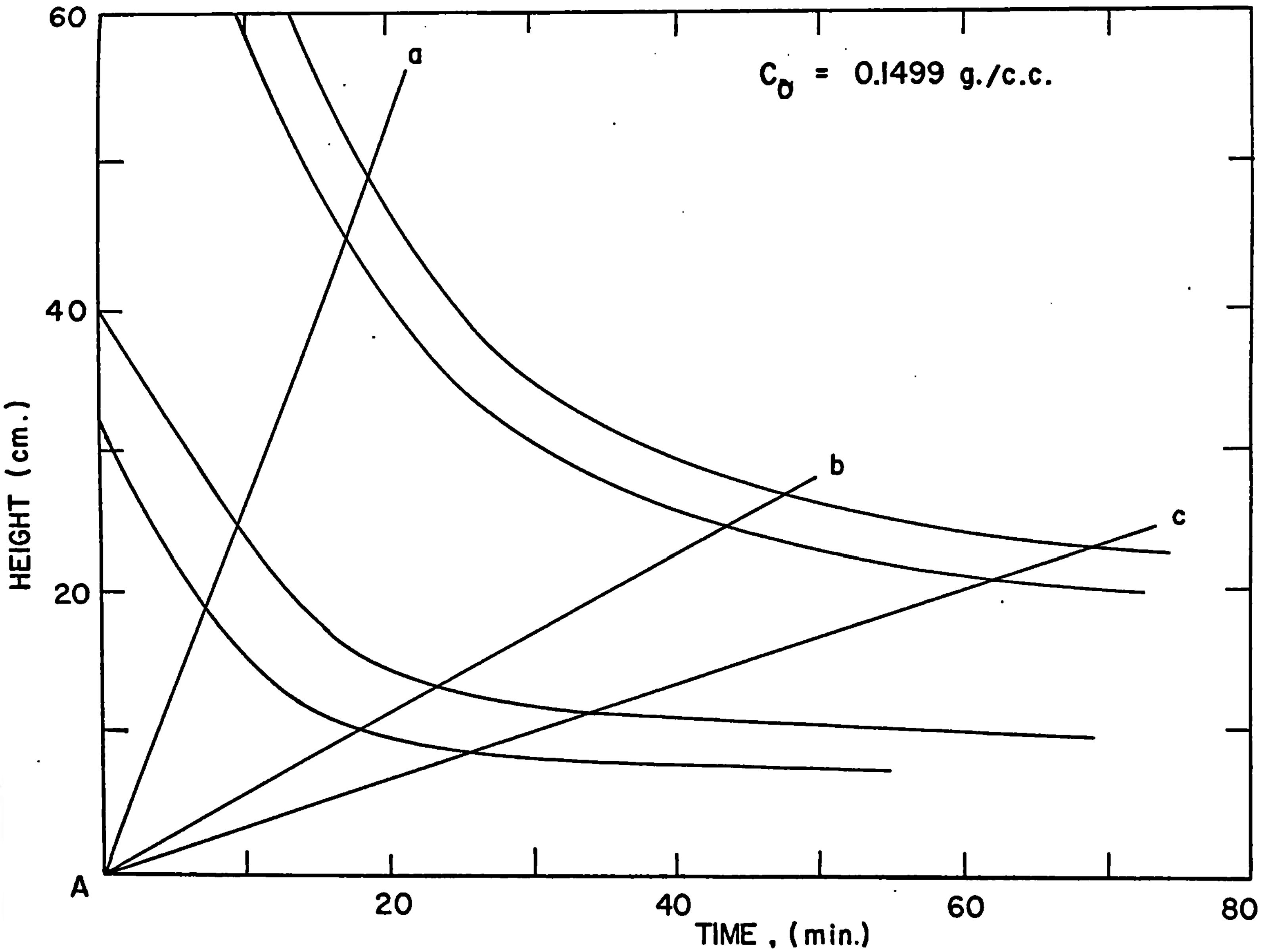

Fig. 9. Geometric Similarity of Settling Curves.

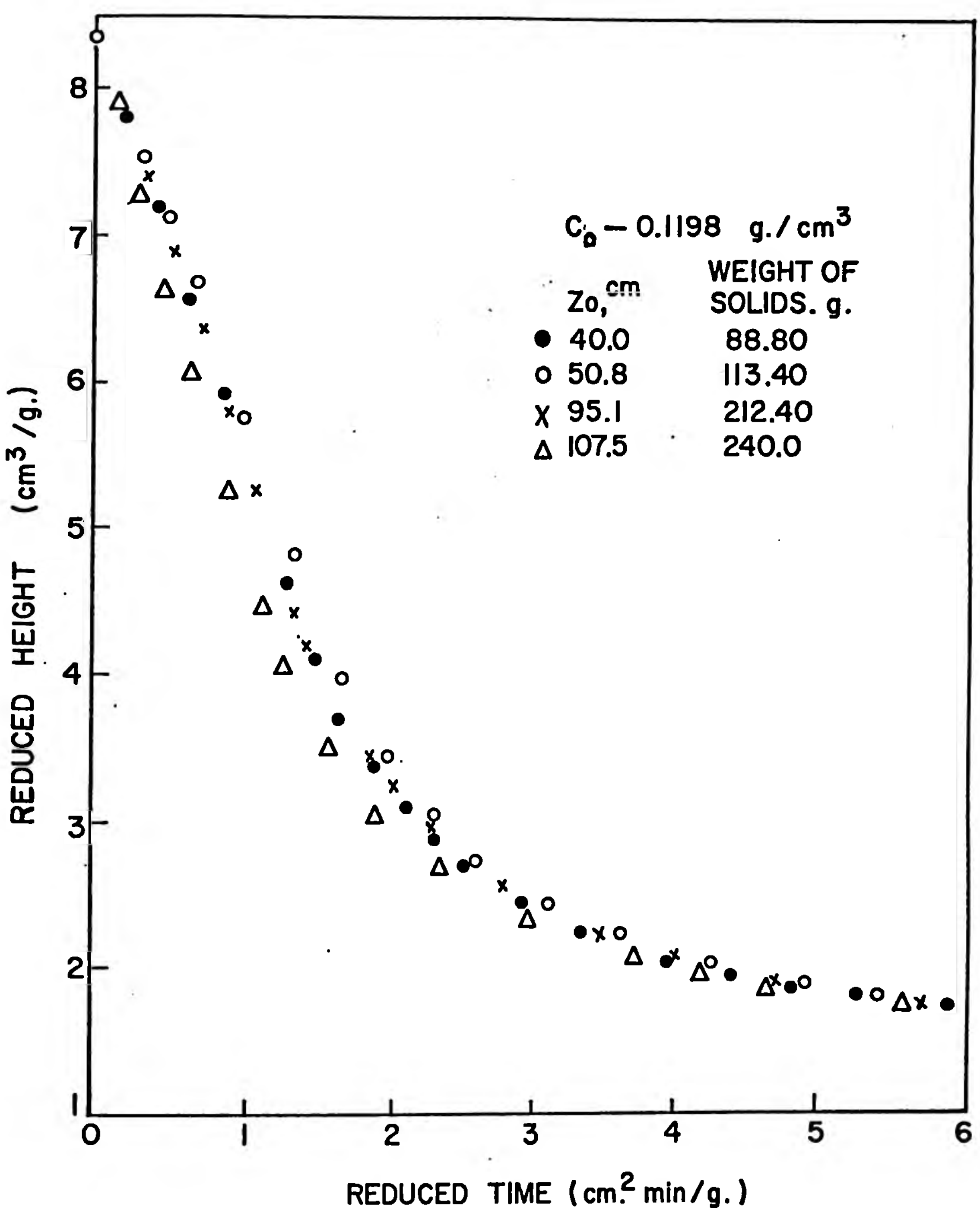

Fig.10 Variation of Reduced Height with Reduced Time.

reduce height vs reduced time plots bear a complementary geometrical relationship. This is exactly similar to Kynch's[20] method of calculating surface concentrations from Equation 14.

Equation 14 assumes that the upward propagation velocity of any concentration is constant. The method of calculating the surface concentration graphically is described below. Let C_o and Z_o be the initial concentration and height, respectively, of a column of slurry in a batch test. When any capacity limiting concentration layer reaches the slurry interface, all solids in the column must have passed through it since it was propagated up from the bottom of the column. If the concentration of this layer is C and it reaches the interface at time t, then the quantity of solids having passed through this layer $CAt\ (u-\delta)$ must equal to the total volume of solids C_oZ_oA. Thus $CtA\ (u-\delta) = C_oZ_oA$ (22)

Since it was proved that the upward velocity of any specific layer is constant.

$$\delta = -Z/t \qquad (22a)$$

where Z represents the height at time t.

Substituting in Equation (21) and simplifying,

$$C = \frac{C_oZ_o}{Z+ut} \qquad (14)$$

The velocity u is equal to-dz/dt at the point on a plot Z vs t (Figure 11) at which the layer having a concentration of C comes to the surface. u is the absolute value of the slope of the tangent to the curve at Z,t. It follows immediately that $Z+ut = Z_{ext}$. Then equation (14) becomes

$$C = \frac{C_oZ_o}{Z_{ext}} \qquad (23)$$

This means that Z_{ext} is the height which the slurry would occupy if all the solids present were at the same concentration as the layer at the slurry

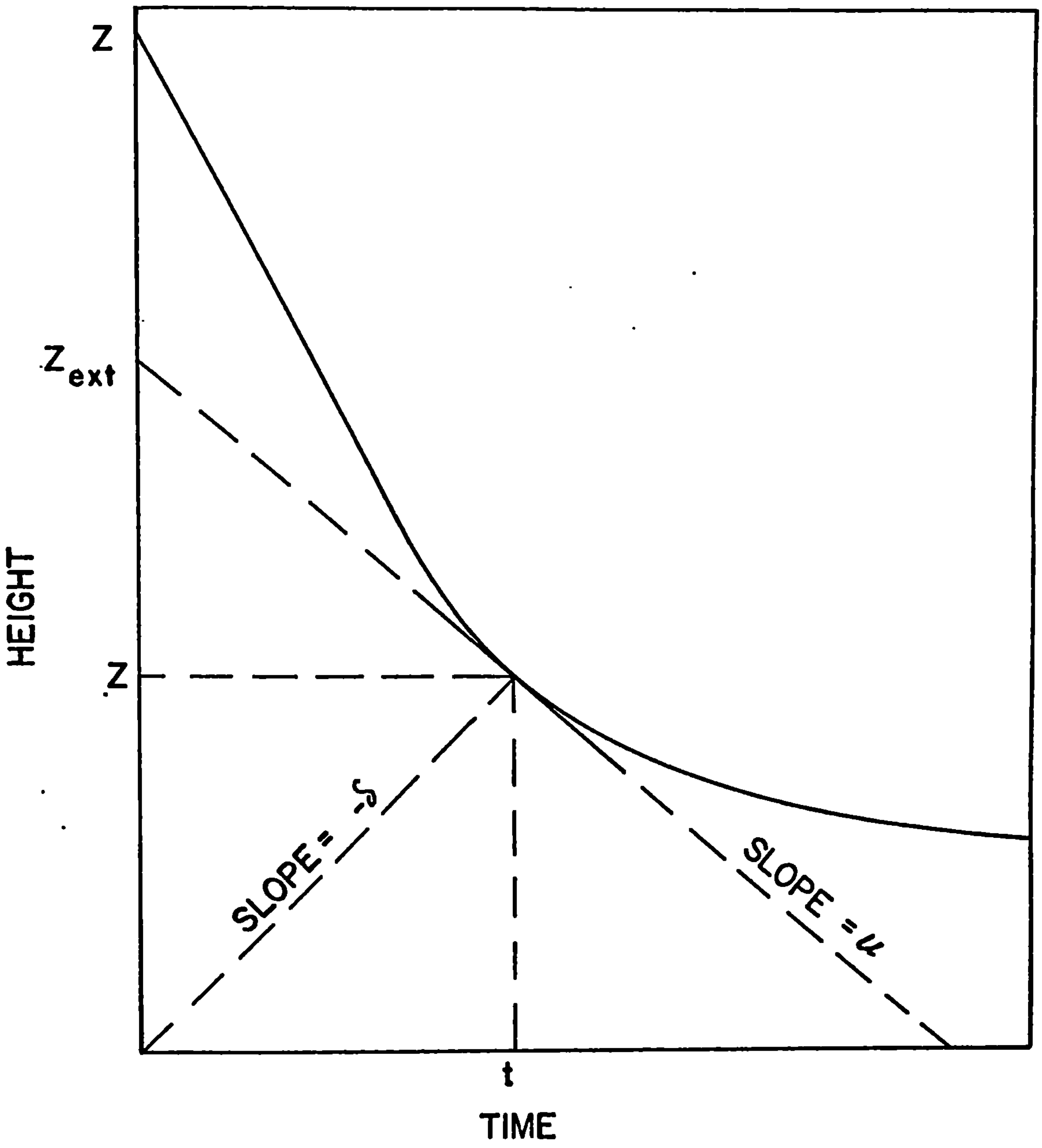

Fig. 11 Determination of Local Solids Concentration.

supernate interface. For any arbitrarily chosen value of C, the corresponding value of Z_{ext} may be calculated, u can then be determined as the slope of the line drawn through the point Z_{ext} and tangent to the settling curve, and a complete set of data showing u as f(c) can therefore be developed from one settling test.

On a reduced plot, by applying the same procedure as above, the intercept on the y-axis gives the value of $\frac{1}{U}$ directly and the intercept on the x-axis gives $\frac{1}{S}$. The advantage of using reduced plot is that, the falling rate period is represented on a single curve for all weights of solids. If weight of solids is a parameter, different curves for different weights will be obtained.

However, in calculating the surface concentrations, Equation 14 was used.

The results are given in a flux plot (Figure 12). Instead of lying on a single curve, they fall in a wide band. Values from six other runs (113.4g., 0.1499 and 0.2400 g./cc; 212.4 g, 0.1499, 0.1917 and 0.2400 g./cc; 240.0g. and 0.1198g./cc) fell between the extremes shown in Figure 12. There is considerable variation from batch to batch and even some variation from run to run, but it appears that the weight of solids has little if any effect on the flux.

An interesting sidelight was that, for two runs, it was possible to fit Roberts equation to the final part of the settling curve. One of them is shown in Figure 13. As these slurries are incompressible, this supports the contention[26] that Roberts equation does not have the significance attributed to it by its author[11].

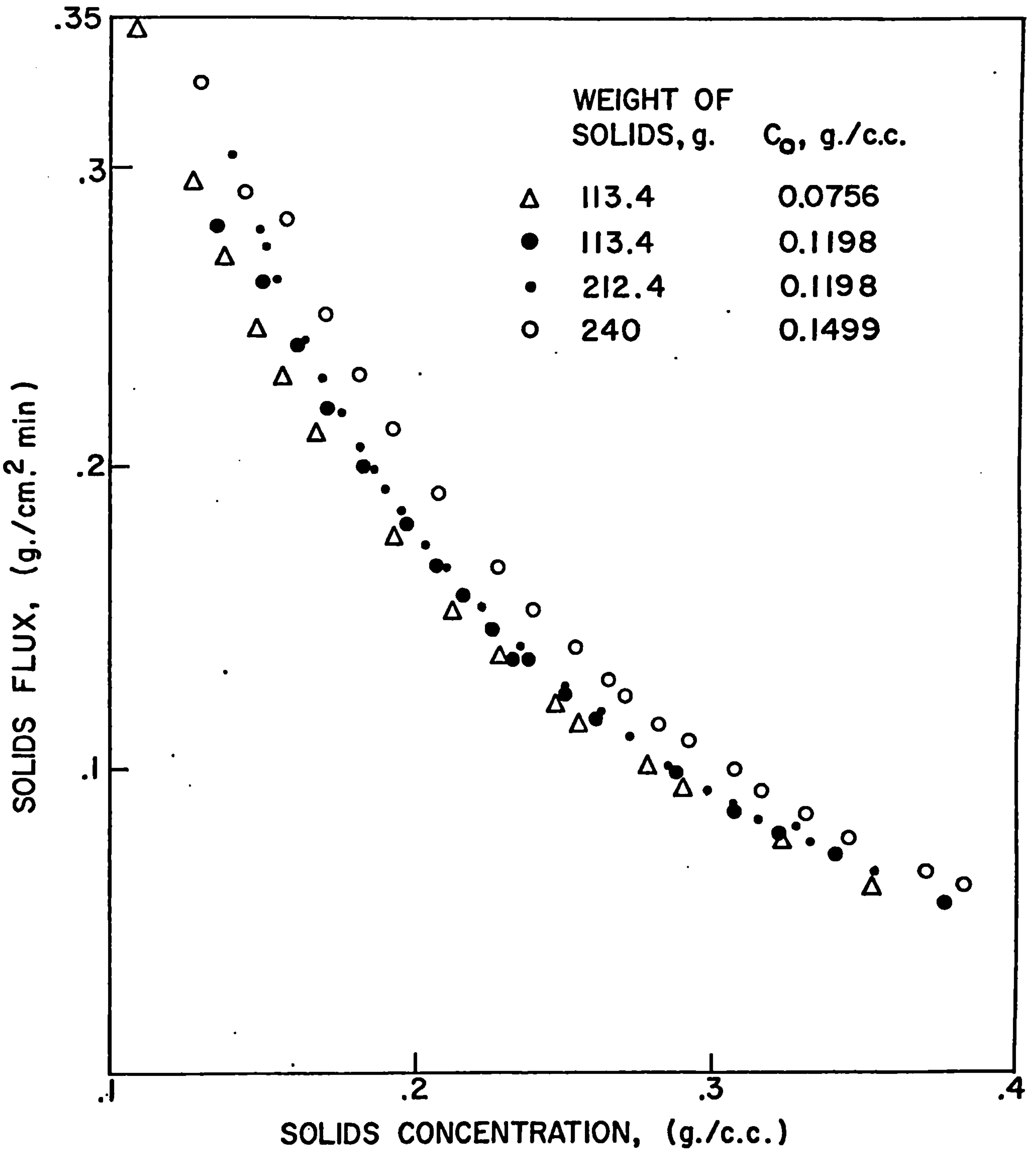

Fig. 12 Variation of Flux with Weight of Solids.

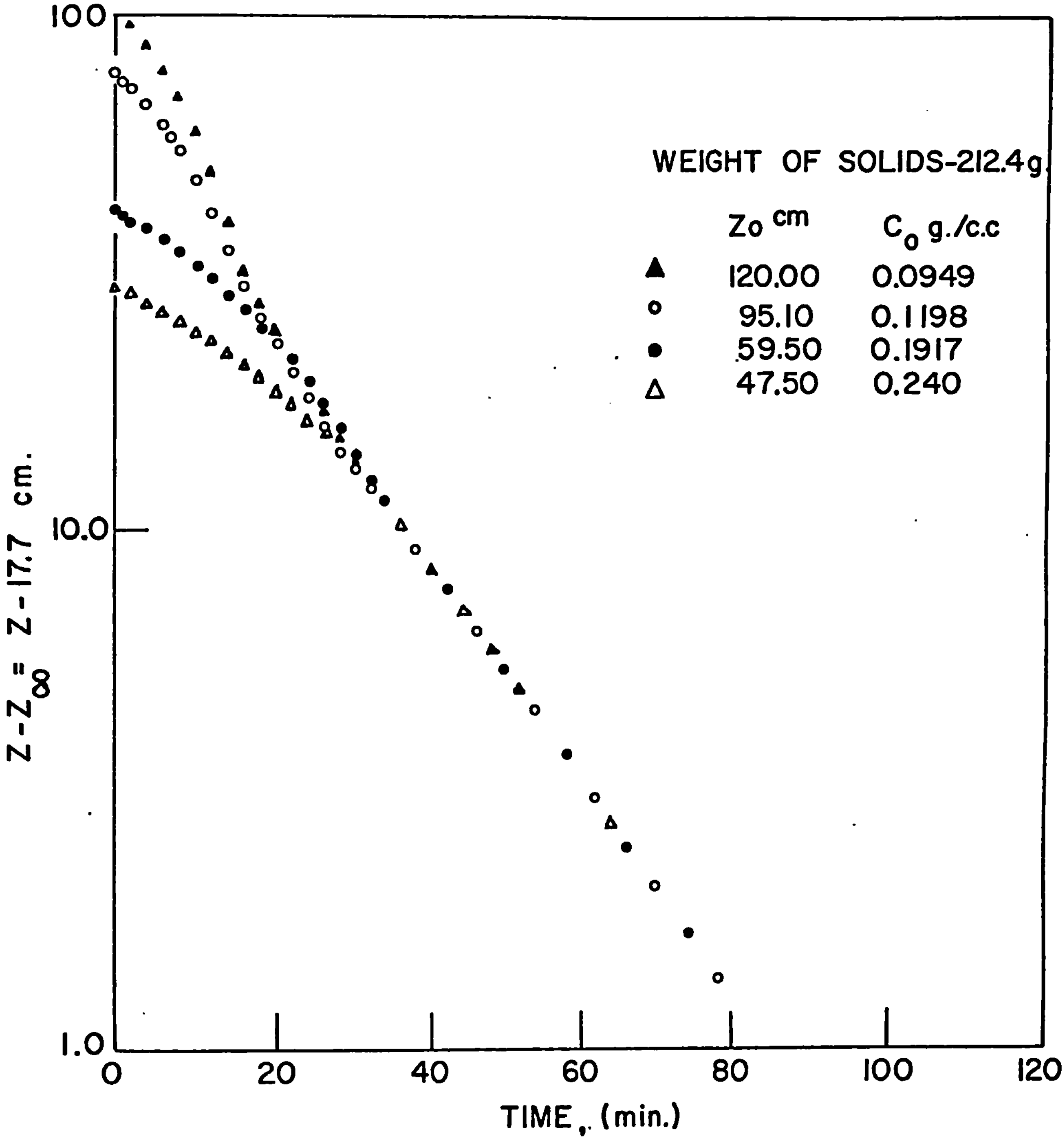

Fig. 13 Application of Roberts' Equation to Final Part of Settling Curve.

INTRODUCTION

The Kynch theory postulates that the rate at which particles settle at any point in a slurry is a function only of the local solids concentration. In applying this theory to slurries in which other factors may also be important, it is necessary to determine the local solids concentration as a function of time and height without causing any disturbance to the system. Ordinary analytical methods fail because samples cannot be withdrawn without disturbing or changing the system to some extent. Attenuation of radiation is one way of determining the solids concentration of thick slurries and both X-rays[31] and gamma rays[26] have been used. This method depends on the difference in absorption coefficients of solid and liquid and the presence of enough solid to affect the amount of absorption.

In very dilute slurries, the amount of solid is not enough to affect the attenuation appreciably, and another method must be found. Richardson and Shabi[32] used radioactive solids in a study of solids remaining in suspension after various periods of time. In some cases, part or all of the material being studied can be made radioactive. Otherwise it is necessary to use a gamma emitter with the same settling properties as that of the substance under investigation.

Certain limitations are immediately apparent. The half-life should be long enough to permit measurements over a reasonable period. If, however, it is very long, there may be a safety or disposal problem.

The material should be readily activated, that is, it should have a fairly large absorption cross section for slow neutrons. As radiation comes from all parts of the slurry, it is necessary to shield the detector. If the gamma radiation is "soft" enough to be absorbed by thin shielding, there may be considerable attenuation by the solid particles. However, for gelatinous slurries in which the actual amount of solid is small, the absorption will be essentially the same as in water. If the gamma radiation is "hard", a good deal of radiation will penetrate the lead and be counted. Nevertheless, it is possible to use this method for emitters of high-energy gamma radiation.

THEORY

A radioactive slurry in a cylindrical container emits gamma radi--ation. A detector is enclosed by a lead shield in which there is a hori-zontal slit. Some of the radiation from a thin cylindrical section of slurry can strike the detector without passing through any lead. Radiation from all parts of the slurry, including this section, can strike the detec-tor by passing through varying thicknesses of lead. Although it is only a fraction of the total radiation, the contribution of the thin cylindrical section of slurry directly in front of the slit will be greater than that of any comparable section. If the shield is properly designed, the contri-bution of a thin section becomes progressively less as the distance from the slit increases. The contribution of a thin cylindrical section of fixed activity is thus a function of the distance from the slit. If z is the position of the centre of the section and x is the position of the centre of the slit, both zero at the bottom of the container and positive upward, this function is $f(z-x)=f(y)$.

Mathematically, $f(y)$ is a known even function (experimentally deter-mined) which is continuous with continuous derivatives.

$$\lim_{y \to \infty} f(y) = 0 \qquad (24)$$

$$\frac{df}{dy} < 0 \qquad \text{for } y > 0 \qquad (25)$$

The solids concentration, $c(z)$, is sectionally continuous. (There may be several finite step changes in $c(z)$).

$$0 \leq c(z) \leq c_o \quad \text{for all } x \tag{26}$$

where c_o is the maximum solids concentration, a finite positive constant. Also,

$\frac{dc}{dz} \leq 0$ for all values of z at which it exists. All step changes are downward with increasing z.

The counting rate when the slit is positioned at x is

$$R(x) = k \int_0^{z_o} c(z)\ f(z-x)\ dz \tag{27}$$

for the case where self-absorption is negligible. Only in this case is $f(z-x)$ independent of $c(z)$. The assumptions about $c(z)$ and $f(z-x)$ guarantee that $R(x)$ is not merely continuous but differentiable(33).

If the concentration is uniform throughout a slurry of height z_o, $R(x)$ is symmetrical about $z_o/2$ and has its maximum value there. Hence, mixing the slurry until its concentration is uniform provides a method of determining the constant k. The other restriction is then

$$\int_0^{z_o} c(z)\ dz = c_o z_o \tag{28}$$

where c_o and z_o are the initial solids concentration and initial slurry height respectively.

A hypothetical example may serve to illustrate the method. Assume that

$$f(z-x) = \frac{1}{1 + (\frac{z-x}{4})^2} \tag{29}$$

A radioactive slurry has an initial height of 48 cm. and an initial concentration of 1/3 g./cc. After a period of settling, the slurry-supernate interface has reached 32 cm. One theory[24] predicts that the solids concentration is 1 g./cc between 0 and 8 cm. and 1/3 g./cc between 8 and 32 cm. The other[22] predicts that the concentration is 1/2 g./cc between 0 and 32 cm. Both are consistent with the material balance and it is desired to use the radioactivity to test them.

For the first theory

$$\frac{R_1(x)}{k} = \int_0^{z_0} \frac{c(z)}{1+(\frac{z-x}{4})^2}\, dz$$

$$= \int_0^{8} \frac{1}{1+(\frac{z-x}{4})^2}\, dz + \int_8^{32} \frac{1/3}{1+(\frac{z-x}{4})^2}\, dz + \int_{32}^{43} (0)\, dz$$

$$= \arctan\left(\frac{8-x}{4}\right) - \arctan\left(-\frac{x}{4}\right) + \frac{1}{3}\arctan\left(\frac{32-x}{4}\right) - \frac{1}{3}\arctan\left(\frac{8-x}{2}\right)$$

$$= \arctan\left(\frac{x}{4}\right) + \frac{2}{3}\arctan\left(\frac{8-x}{4}\right) + \frac{1}{3}\arctan\left(\frac{32-x}{4}\right) \qquad (30)$$

For the second theory

$$\frac{R_2(x)}{k} = \int_0^{z_0} \frac{1/2}{1+(\frac{z-x}{4})^2}\, dz$$

$$= 1/2 \arctan\left(\frac{32-x}{4}\right) - 1/2 \arctan\left(-\frac{x}{4}\right)$$

$$= 1/2 \arctan\left(\frac{x}{4}\right) + 1/2 \arctan\left(\frac{32-x}{4}\right) \qquad (31)$$

Now consider the values of $\frac{R(x)}{k}$ at 0, 4, 8, 16, 24, and 32. These are given below along with pertinent values of the arctangent.

x	$\arctan(\frac{x}{4})$	$\arctan(\frac{8-x}{4})$	$\arctan(\frac{32-x}{4})$	$\frac{R_1(x)}{k}$	$\frac{R_2(x)}{k}$
0	0	1.1072	1.4464	1.2202	0.7232
4	0.7854	0.7854	1.4289	1.7853	1.1131
8	1.1072	0	1.4056	1.5757	1.2564

x	arctan $(\frac{x}{4})$	arctan $(\frac{[illegible]}{4})$	arctan $(\frac{[illegible]}{4})$	$\frac{R_1(x)}{k}$	$\frac{R_2(x)}{k}$
16	1.3258	-1.3072	1.[illegible]	1.0295	1.3[illegible]50
24	1.4056	-1.3258	1.1[illegible]72	0.8[illegible]8	1.2564
32	1.4464	-1.4056	0	0.5095	0.7252

In practice, $f(z-x)$ will be available only as a calibration curve, and $c(z)$ may be more complicated. However, an estimate of $c(z)$ can be made from the settling curve by applying [illegible]'s theory. If this estimate does not agree with the experimental values, the size and distribution of the disparities will indicate where adjustments should be made. The new estimate must, of course, satisfy all the limitations on $c(x)$.

The counting rate $R(x)$ is a transform of the concentration $c(z)$ and the calibration curve $f(z-x)$ is the kernel of the transform. The problem of finding $c(z)$ when $R(x)$ is known is simply that of finding the inverse transform. The nature of the functions $c(z)$ and $f(z-x)$ ensures that when $R(x)$ is known, $c(z)$ is determined uniquely except where it is discontinuous.

EXPERIMENTAL

Materials

After careful study, it was decided to use praseodymium oxalate as the radioactive substance. A small sample from Lindsay Chemical Division permitted a study of its settling characteristics and the characteristics of the radioactive isotope Pr^{142} for which the decay scheme is

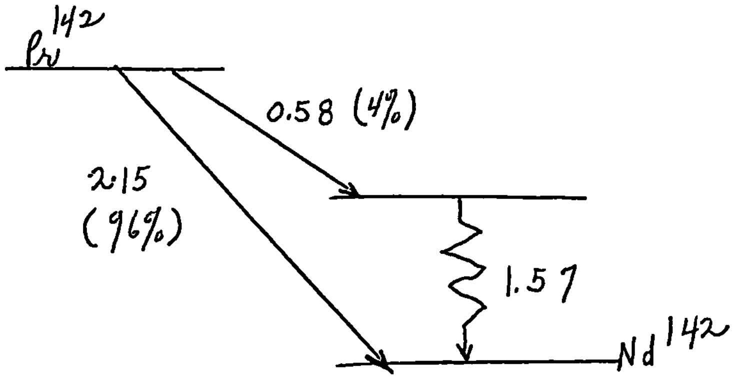

Except for its very high energy gamma (1.57 Mev) and its low (4%) decay by gamma radiation, it was satisfactory in all respects. The hard gamma did eliminate the need to consider self absorption and the large amount of beta radiation presented no problems.

The settling characteristics of this suspension are very interesting in that they are intermediate between those for rigid spheres and flocculated compressible slurries. Reproducibility with the same batch is good, but for different batches it depends upon age, agitation, and possible other factors. The main interest in the present problem is to test Kynch's hypothesis and determine its limitations. The reproducibility does not affect our analysis since calculations can be done for each run separately. The preparation of the slurry was described in Part I.

Apparatus and Procedure

The apparatus was designed to permit measurements of concentration to be made over a period of time at any depth in the sedimenting suspension. For reasons of safety the sedimenting column was enclosed by a glass walled water jacket to absorb the β particles. It was so arranged that all the operations could be done without direct contact with the active material.

Because of the weight of the heavy lead shielding surrounding the detector, the measuring equipment was fixed in position and the vessel containing the suspension was arranged so that it could be raised or lowered inside the water shielding. Sedimentation was carried out in a pyrex glass column 4.9 cm in diameter (I.D.) and 80 cm long. The rate of fall of the sludge line could be easily observed despite the water jacket surrounding the settling column.

A known weight of the material was transferred into the column in the form of a slurry. A much smaller known weight was placed in a polythene capsule and irradiated in a flux of 3×10^{12} neutrons/cm^2. The irradiated capsule was transported by means of a rabbit system to the "hot lab". The contents of the capsule were transferred into a beaker and thence into the settling column. Long tongs were used in all these operations with radioactive materials.

The settling column was moved up and down with a pulley arrangement and the slurry was mixed uniformly by means of a plunger which was fixed in line with the column (Figure 14). The settling column was then fixed at any desired level and the counting started.

Radiation from the bulk of the slurry was attenuated by a lead

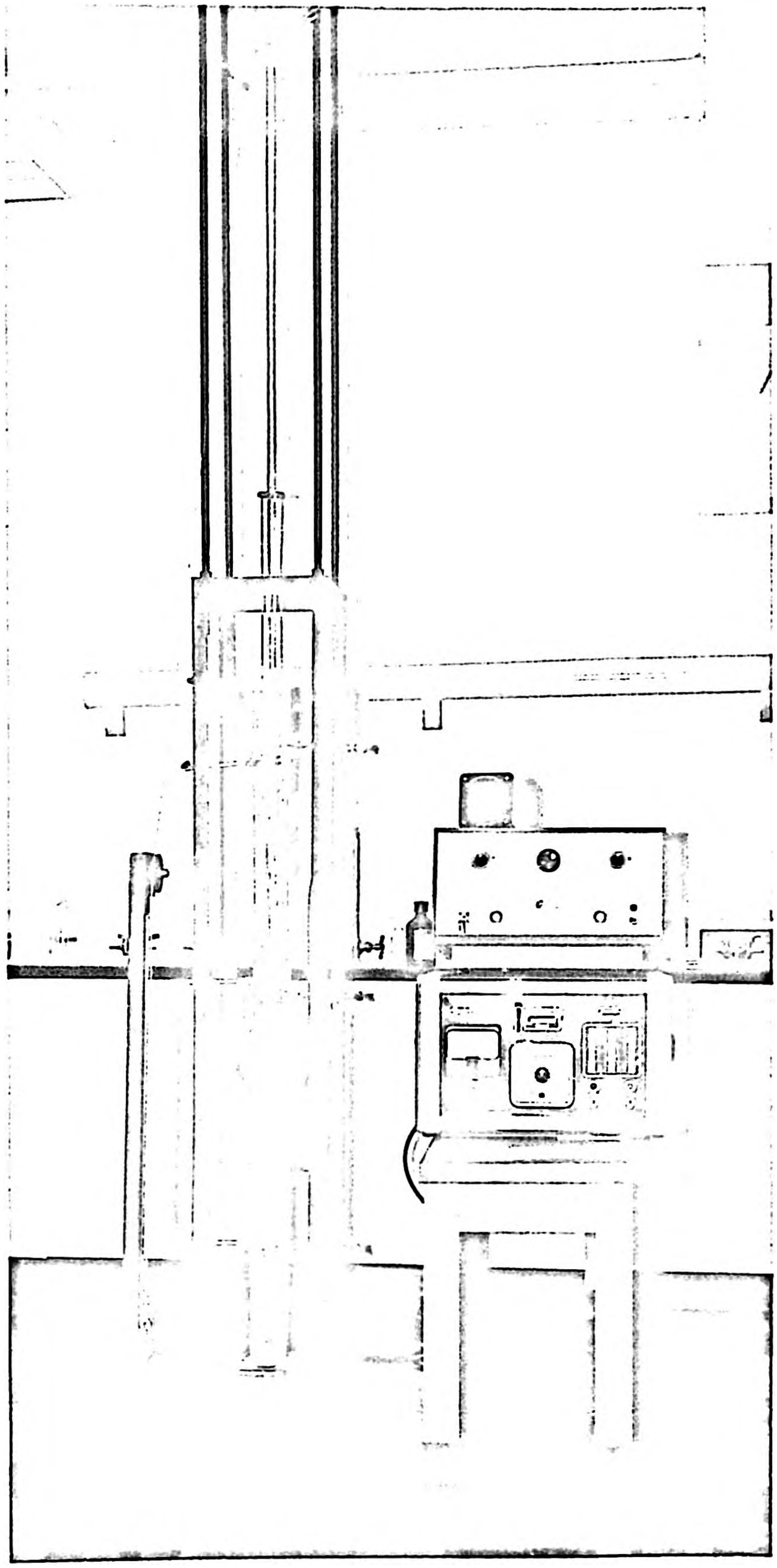

Fig. 14 Experimental Apparatus

Fig. 15 Detail of Experimental Apparatus

shield in approximately the form of a thick-walled cylindrical tank laid on its side. The top view is shown below.

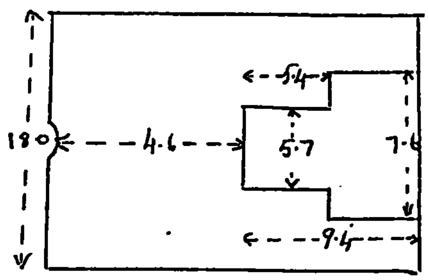

A thin horizontal slit (0.318 cm. by 1.90 cm) permitted unimpeded entry of some of the radiation from a very short depth of slurry. The geometry of the system is complex, but rough estimates are made in Appendix C of view factors and the expected amounts of radiation coming through the slit and through the lead respectively.

The detector, which was placed inside the shield was a NaI (Tl) scintillation crystal (Harshaw, Type 8D8P4). The measuring equipment consisted of radiation analyzer (Nuclear Chicago, Model 1810) and a scaler (Tracerlab Inc., Model 1000). The length of counting time was set by a timer (Nuclear Instrument and Chemical Corp., Model T1).

RESULTS

The most obvious way to measure the solids concentration is to attempt to shielf the detector from all radiation except that emanating from a thin cylindrical section directly in front of the slit. Approximate values of the view factor were calculated for various thicknesses of shielding and slit dimensions (Appendix C). In addition, estimates were made of the effect of radiation emanating from other parts of the slurry. For the example shown in Appendix C, the "desired" radiation constituted only 8.7% of the total. These estimates showed that while the "extraneous" radiation decreased sharply with increasing thickness of shielding, the "desired" radiation decreased considerably. The gain in percent "desired" radiation was offset by decreased counting accuracy.

A thin cylindrical section of highly radioactive (5 mc) slurry gave the calibration curve shown in Figure 16. The shielding design was satisfactory in that it produced a monotonically decreasing calibration curve. The thick shielding around the lateral surface of the scintillation crystal reduced the effect of radiation emanating from intermediate distances while the moderate thickness directly in front ensured that the contribution of the radioactive material there was considerably higher than from anywhere else. Although the calibration curve was satisfactory, only 5.5% of the radiation received from an infinite column came from the volume of slurry "seen" by the detector through the slit. However, it should be emphasized that the function of the shielding in the present method is not to shut out all "extraneous" radiation but to provide a suitable kernel, $f(z-x)$, for the transformation $R(x) = k \int_0^{z_0} f(z-x)\, c(z)\, dz$.

A thin cylindrical section of slurry with an activity of 5 mc. produced about 240,000 counts per minute when directly in front off the slit. The theoretical value, which involved numerous approximations and estimates was 2?0,000 (Appendix C). This gives hope that the theoretical method, despit its roughness, will be useful in estimating results for other radioactive isotopes.

To gain facility in handling radioactive materials and to test the feasibility of the method, a number of preliminary settling tests were done with slurries ranging in activity from 0.2 to 1 mc. These indicated that an activity of 5 mc. would be necessary to obtain good counting accuracy.

A test of Kynch's theory was made with 216.6 g of praseodymium oxalate having an activity of roughly 5 mc. The concentration at different levels in the slurry was calculated from the settling curve[21] on the basis of Kynch's theory that concentration changes are propagated upwards with a constant velocity[20]. This lead to the theoretical distributions shown in Figure 17. From the values of $f(z-x)$ in Figure 16 and $c(z)$ in Figure 17, the value of $R(x)/k$ was determined by a numerical integration using an increment of 0.4 cm. The value of k was determined from the known initial concentration. The theoretical counts were then compared to the experimental.

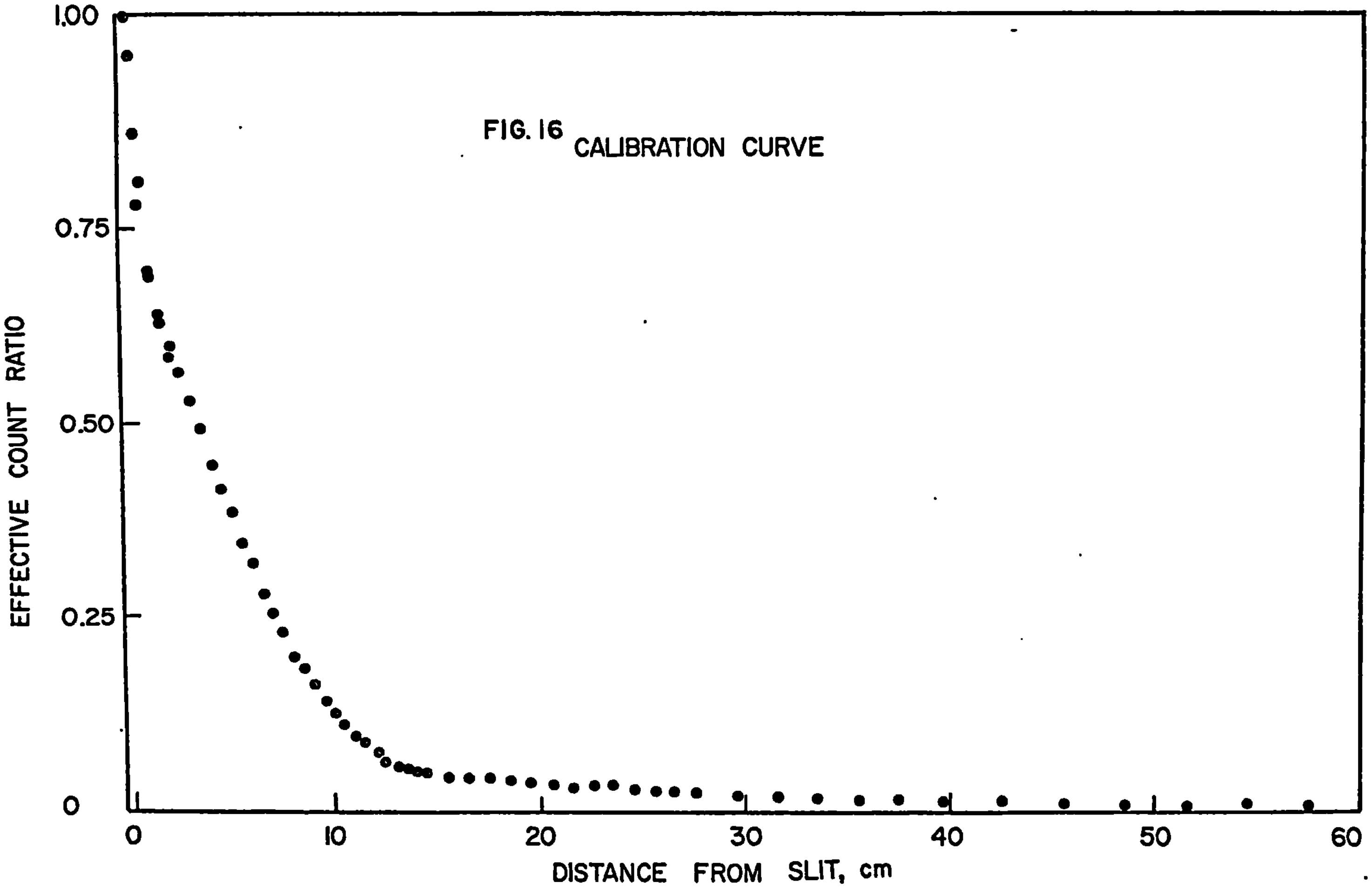

FIG. 16 CALIBRATION CURVE

23

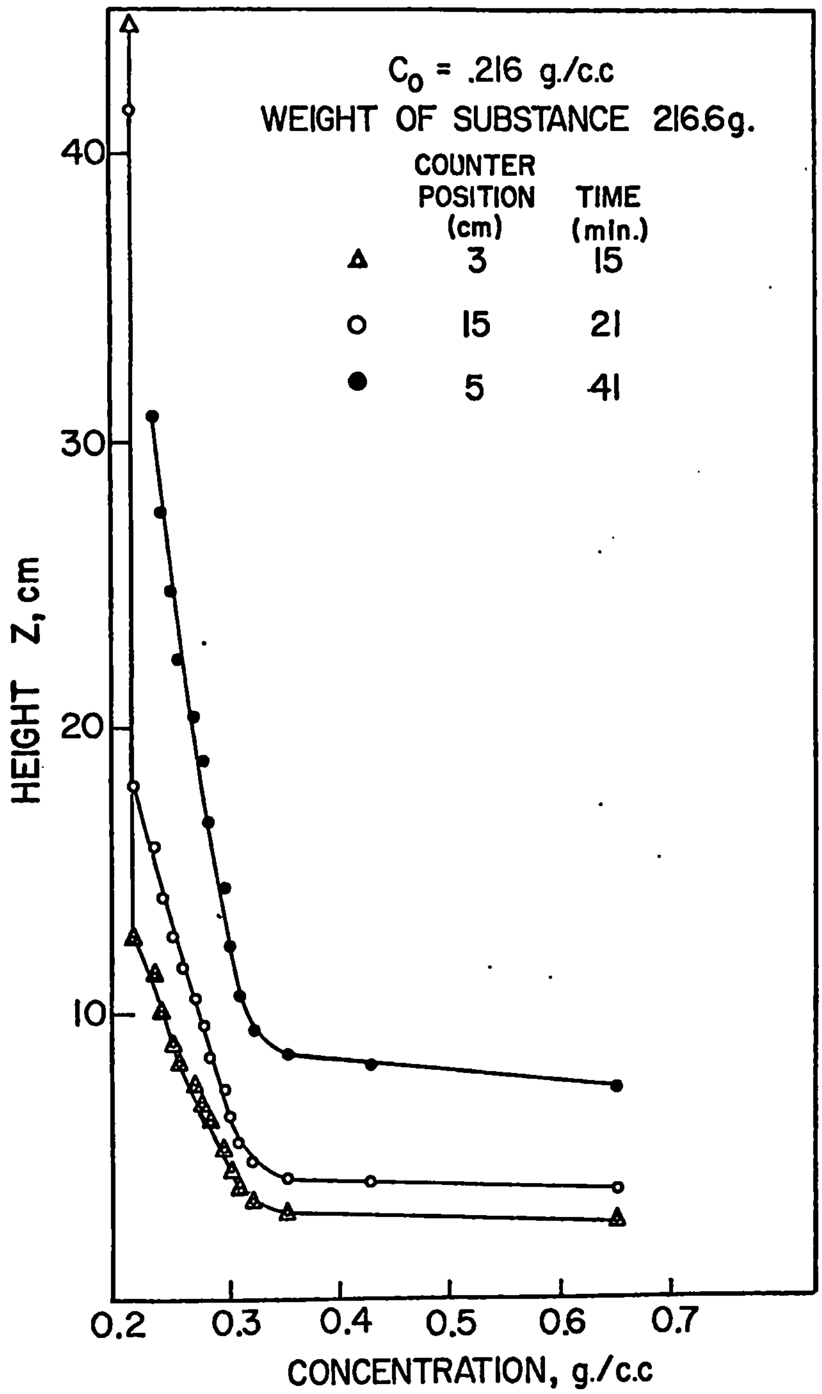

Fig. 17 Concentration Distribution as a Function of Time.

TABLE 5

Comparison of Theoretical and Experimental Counting Rates

Slit Position (cm)	Interface Level (cm)	Time (min)	Counts per Minute Calculated	Counts per Minute Observed	Diff. (%)
3	44.6	15	20,400	18,984	7.5
15	41.4	21	17,493	17,523	0.5
5	30.9	41	30,840	27,800	10.9

For a slit position of 15 cm., the agreement is perfect, indicating that the solids concentration remains constant except in the lower portion of the slurry. The failure of the calculated and observed counts to agree completely at low slit positions indicates that a concentration gradient exists in the settled bed. This was confirmed by taking counts over the height of the slurry when settling was complete. Instead of being symmetrical about the midpoint, the distribution was biased towards the bottom. Based on the average of the two appropriate values, the disparity was 2.2% for values ± 3.5 cm. from the midpoint and 18.5% for ± 8.25 cm.

Further development of the method depends upon the development of a computer programme which will utilize an iterative procedure to calculate the experimental concentration from the observed counting rate at a number of points. This appears to be feasible. The theoretical concentration distribution is an excellent first estimate, differing only in the region of the packed bed, and here the direction of the deviation is obvious.

APPENDIX A

(Tables 6-11)

TABLE 6

Batch 1

Initial Settling Rates vs. Initial Concentration

Weight of Solids 88.8 g. Temperature 27-28^{o}C

Height Z_o (cm)	Concentration C_o (g./cc)	Void fraction	Rate of settling u (cm/min)
15.0	0.320	0.8728	0.328
			0.3472
20.0	0.240	0.9048	0.650
			0.650
25.0	0.1914	0.9240	1.050
			1.00
32.0	0.1486	0.9410	1.950
			1.922
40.0	0.1190	0.9528	3.10
			3.16
50.0	0.0950	0.9623	4.45
			4.75
63.0	0.0757	0.970	6.60
			6.50
80.0	0.0595	0.9734	8.517
			8.286
100.0	0.0476	0.9811	10.50
			9.50

Height Z_o (cm)	Concentration C_o (g./cc)	Void fraction	Rate of settling u (cm/min)
120.0	0.0396	0.9842	11.50
			11.50

TABLE 7

Batch 2

Initial Settling Rates vs. Initial Concentrations.

Weight of Solids 240.0 g.   Temperature 26-29°C

Height Z_o (cm)	Concentration C_o (g/cc)	Void fraction	Rate of settling u (cm/min)
25.2	0.5140	0.7957	0.0744
			0.0709
29.0	0.4445	0.8237	0.1122
			0.1060
32.0	0.4028	0.8403	0.[illegible]28
			0.200
40.3	0.320	0.8731	0.3580
			0.360
53.7	0.240	0.9048	0.640
			0.635
67.2	0.1917	0.924	1.0190
			1.047
86.0	0.1499	0.9405	2.025
			2.025
107.5	0.1198	0.9525	3.650
			3.650
120.0	0.1073	0.9574	4.72
			4.75

TABLE 8

Batch 3

Initial Settling Rates vs. Initial Concentration

Weight of Solids 113.4 g.   Temperature 27-29.5°C

Height Z_o (cm)	Concentration C_o (g./cc)	Void fraction ε	Rate of settling u (cm/min)
13.70	0.4445	0.8237	0.10 0.10
15.10	0.4028	0.8403	0.1347
19.00	0.320	0.8731	0.328 0.318
25.40	0.240	0.9048	0.6149 0.6149
31.70	0.1917	0.9240	0.945
40.60	0.1499	0.9405	1.70
50.80	0.1198	0.9525	2.95 2.85
56.70	0.1073	0.9574	3.776 3.60
64.0	0.0949	0.9623	4.60 3.90
80.40	0.0756	0.970	6.50 6.235
102.10	0.0595	0.9764	7.97 7.25
120.00	0.05072	0.9799	9.50 8.50

TABLE 9

Batch 4

Initial Settling Rates vs. Initial Concentrations

Weight of Solids 212.4 g. Temperature 25-28°C

Height Z_o (cm)	Concentration C_o (g./cc)	Void fraction ε	Rate of settling u (cm/min)
22.30	0.514	0.7957	0.0589
			0.060
25.60	0.4445	0.8237	0.150
			0.1367
28.30	0.4028	0.8403	0.20
			0.20
35.60	0.320	0.8731	0.328
			0.335
47.50	0.240	0.9048	0.5718
			0.5587
59.50	0.1917	0.9240	0.9333
			0.9250
76.10	0.1499	0.9405	1.95
			2.00
95.10	0.1198	0.9525	3.280
			3.200
106.20	0.1073	0.9574	3.95
			4.15

TABLE 11

Batch 6

Initial Settling Rates vs. Initial Concentration

Weight of Solids 159.0 g.   Temperature 26-28°C

Height Z_o (cm)	Concentration C_o (g./cc)	Void fraction ε	Rate of Settling u (cm/min)
39.0	0.240	0.9048	0.460
			0.450
48.8	0.1917	0.924	0.70
			0.72
52.0	0.180	0.9286	0.80
			0.80
55.0	0.170	0.9326	0.85
			0.95
62.4	0.1499	0.9405	1.10
			1.25
78.0	0.1198	0.9525	1.950
			2.00
87.2	0.1073	0.9574	2.70
			2.95

APPENDIX B

Determination of Slurry Concentration

The apparent density of Pr oxalate was determined by adding a known amount of Pr oxalate to a 500 ml volumetric flask and adding water to give a total volume of 350-450 ml. The flask was then stoppend and shaken vigorously. Agitation was repeated for a long time at frequent intervals. The flask was then opened, the slurry was washed down from the walls, and kept in a constant temperature bath at 20°C. Finally water was added up to the mark. Since the volume of water and total volume is known, the apparent density of Pr oxalate in water can be calculated. The density determined from slurries of 0.1 000 g./cc was too low when compared to 0.200 g/cc - 0.6100 g./cc slurries and was discarded. The results for these slurries are shown in the following table.

Weight of Pr oxalate(g)	Weight of Water (g)	Volume of Water (cc)	Volume of Pr Oxalate (cc)	Density of Pr Oxalate (g/cc)
122.659	450.6325	451.4304	48.5696	2.5254
112.4505	454.6995	455.5046	44.4954	2.5272
129.0345	448.075	448.8684	51.1316	2.5235
163.739	434.552	435.3215	64.6785	2.5315
153.831	438.143	438.9183	61.0812	2.5184
120.2945	451.2335	452.0385	47.9615	2.5081
208.1275	416.6935	417.4313	82.5687	2.5206

$$\Sigma p_i^2 = 44.529276$$

$$(\Sigma p)^2/7 = 44.52888$$

The estimated standard deviation of Mean $= \sqrt{\dfrac{\Sigma p_i^2 - (\Sigma p)^2/n}{(n-1)(n)}}$

$$= \sqrt{0.000396/(6)(7)} = 0.0030708$$

95% confidence limit $\bar{\rho} = 2.522 \pm 0.0075$ g/cm^3

APPENDIX C

Design of Shield for Scintillation Counter

1. Approximate Calculation of View Factors

Disregarding for the moment, the appreciable gamma radiation which penetrates lead shielding, a column of radioactive material separated from a counter in which there is a narrow horizontal slit may be regarded as a short cylinder containing a uniform distribution of sources.

Consider a thin plate source of thickness t.

S = source strength per unit volume

μ = absorption coefficient in source medium

At point P (34)

$$dI = \frac{St}{4\pi r^2} \quad r\, d\phi dr\; e^{-\mu(r-S_1)} \tag{A.1}$$

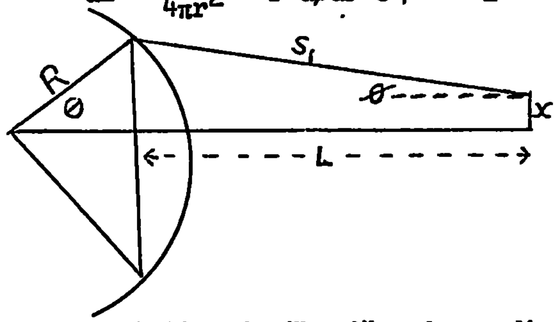

If the gamma radiation is "hard" and the distance $(r-S_1)$ through which it must pass is small, this equation becomes approximately

$$dI = \frac{St}{4\pi} \; \frac{dr}{r}\, d\phi \tag{A.2}$$

The limits on r are S_1 and S_2. Thus,

$$I = \frac{St}{4\pi} \int_{-\arctan\frac{w+x}{L}}^{\arctan\frac{w-x}{L}} \left[\int_{S_1}^{S_2} \frac{dr}{r} \right] d\phi$$

$$= \frac{St}{4\pi} \int_{-\arctan \frac{w+x}{L}}^{\arctan \frac{w-x}{L}} \ln \frac{S_2}{S_1} \, d\phi \qquad (A.3)$$

where w is the half width of the slit.

Both S_2 and S_1 can be expressed as functions of ϕ and x. The two equations for S_1 are

$$x + S_1 \sin\phi = R \sin \theta \qquad (A.4)$$

$$S_1 \cos \phi + R \cos \theta = L + \sqrt{R^2 - w^2} = K \qquad (A.5)$$

From equation A.4

$$R \cos \theta = \sqrt{R^2 - (x + S_1 \sin \phi)^2} \qquad (A.6)$$

Substitution of Equation 6 into Equation (A.5) gives, after some manipulation, a quadratic equation with the solution

$$S_1 = K\cos \phi - x \sin \phi \pm \sqrt{(x \sin\phi - K \cos\phi)^2 - (K^2 + x^2 - R^2)} \qquad (A.7)$$

The two equations for S_2 are

$$x + S_2 \sin \phi = R \sin \theta \qquad (A.8)$$

$$S_2 \cos \phi = K + R \cos \theta \qquad (A.9)$$

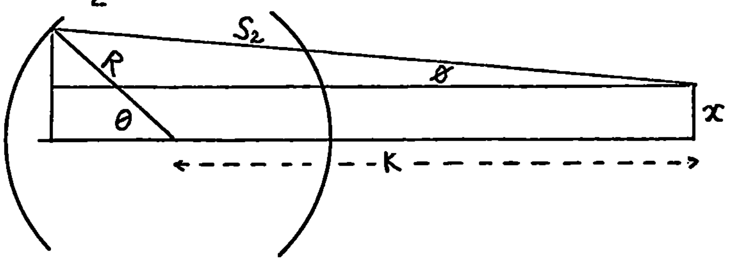

Solution of these equations leads to the same value as that given for S_1 in Equation A.7 As $S_2 > S_1$, the solution is obviously

$$\frac{S_2}{S_1} = \frac{1 + \sqrt{1 - \frac{k^2 + x^2 - R^2}{(K \cos \phi - x \sin \phi)^2}}}{1 - \sqrt{1 - \frac{k^2 + x^2 - R^2}{(K \cos \phi - x \sin \phi)^2}}} \qquad (A.10)$$

For small values of ϕ, $\cos \phi \simeq 1 - \frac{1}{2}\phi^2$, $\sin \phi \simeq \phi$. Hence

$$\sqrt{1-\frac{K^2+x^2-R^2}{(K\cos\phi - x\sin\phi)^2}} \simeq \sqrt{1-\frac{K^2+x^2-R^2}{K^2(1-\frac{1}{2}\phi^2-\frac{x}{K}\phi)^2}} \qquad (A.11)$$

The largest absolute values of ϕ occur when x is of opposite sign. Thus the maximum values of $x\phi/K$ and $\frac{1}{2}\phi^2$ are of opposite sign, and the approximation

$$\frac{1}{(1-\frac{1}{2}\phi^2-\frac{x}{K}\phi)^2} \simeq 1+\phi^2+\frac{2x}{K}\phi \qquad (A.12)$$

is somewhat better than might be thought. Now

$$-\frac{K^2+x^2-R^2}{K^2} = -\left(1-\frac{R^2-x^2}{K^2}\right) \qquad (A.13)$$

and

$$\sqrt{1-\frac{K^2+x^2-R^2}{K^2(1-\frac{1}{2}\phi^2-\frac{x}{K}\phi)^2}} \simeq \sqrt{1-\left[1+\phi^2+\frac{2x}{K}\phi+\frac{x^2}{K^2}-\frac{R^2}{K^2}\right]}$$

$$= \sqrt{\left(\frac{R}{K}\right)^2-\left(\phi+\frac{x}{K}\right)^2} \qquad (A.14)$$

This is of the form $\sqrt{a^2-v^2}$. Thus

$$\ln\frac{S_2}{S_1} = \ln\left(1+\sqrt{a^2-v^2}\right) - \ln\left(1-\sqrt{a^2-v^2}\right) - 2\sqrt{a^2-v^2}\left[1+\frac{1}{3}(a^2-v^2)\right]$$
(A.15)

The value obtained from a table of integrals is, after rearrangement,

$$\int \ln\frac{S_2}{S_1}\,d\phi = \left(1+\frac{1}{4}a^2\right)v\sqrt{a^2-v^2} + \left(1+\frac{1}{4}a^2\right)a^2\arcsin\frac{v}{a}+\frac{v}{6}\sqrt{(a^2-v^2)^3}$$
(A.16)

In terms of the original variables

$$\int_{-\arctan \frac{w-x}{L}}^{\arctan \frac{w-x}{L}} \ln \frac{S_2}{S_1}\, d\phi = \Bigg[\left\{1 + \frac{1}{4}\left(\frac{a}{R}\right)^2\right\}\left(\phi + \frac{x}{R}\right)\sqrt{\left(\frac{a}{R}\right)^2 - \left(\phi + \frac{x}{R}\right)^2}$$

$$+ \left\{1 + \frac{1}{4}\left(\frac{a}{R}\right)^2\right\}\left(\frac{a}{R}\right)^2 \arcsin\left(\frac{\phi + \frac{x}{R}}{\frac{a}{R}}\right) + \left(\frac{\phi + \frac{x}{R}}{6}\right)\sqrt{\left\{\left(\frac{a}{R}\right)^2 - \left(\phi + \frac{x}{R}\right)^2\right\}^3}\ \Bigg]_{-\arctan \frac{w-x}{L}}^{\arctan \frac{w-x}{L}}$$

(A.17)

In Equation A.3, I is the intensity of radiation. Equation A.17, when multiplied by $S_0/\pi a$ gives this intensity as a function of x. To determine the radiation reaching the counter, it is necessary to integrate over the width and thickness of the slit. In the present simplified treatment, the integration is done numerically over the width, and the thickness is introduced separately.

The right hand side of Equation A.17 was used as the integrand in the integration with respect to x between the limits -w and w. The integration utilizing Gauss's quadrature formula, was done on a Bendix G-15 digital computer. The Algo program is given below.

[illegible] 2

1. Title radiation

2. Library arctn (0100000)

3. Data B(9), C(9), x(9), P(9), Q(9), u(9), s(9), v(9), T(9)

4. Subscripts j

5. Constants G(9), A(9)

6. - 0.00016

```
7.    - 0.83603
8.    - 0.61337
9.    - 0.32425
10.   0.00000
11.   0.32425
12.   0.61337
13.   0.83603
14.   0.96816
16.   0.081274
17.   0.18065
18.   0.26061
19.   0.31235
20.   0.33024
21.   0.31235
22.   0.26061
23.   0.18065
24.   0.081274
25.   Begin
26.   R = Keybd.
27.   M = Keybd
28.   N = Keybd
29.   F = Keybd
30.   Y = Keybd
31.   Z = Keybd
32.   E = Keybd
33.   For W=Y(Z) E begin
```

```
34.     Print (FL) = W

35.     Carr (1)

36.     For K=H(H)F Begin

37.     Tabs (1)

38.     Print (FL) = K

39.     Tabs (1)

40.     D = 0

41.     L=F-SQRT (R↑2-W↑2)

42.     For J=0(1)8 Begin

43.     X [J] = W*G [J]

44.     P [J]= - Arctn ((L+X [J] )/K)

45.     Q [J]=   Arctn ((L-X [J] )/K)

46.     T [J]= (P [J] + X [J] /K)*K/R

47.     U [J]= (Q [J] +X [J] /K)*K/R

47.1    TT=ABS(T [J])

48.     S [J] = T [J] *(1+TT↑2/6+3*TT↑4/40+15*TT↑6/336) UU=ABS(U [J] )

49.     V [J] = U [J] *(1+UU↑2/6+3*UU↑4/40+15*UU↑6/336)

50.     B [J] = (1+(R/K)↑2/4)*(P [J] +X [J] /K)*SQRT((R/K)↑2-(P[J]+X[J]/K)↑2)
                  +(1+(R/K)↑2/4)*(R/K)↑2*S [J]
                  +(P [J] +X [J] /K)*SQRT(((R/K)↑2-(P[J]+X [J]/K ↑2)↑3)/6

51.     C [J] =(1+(R/K)↑2/4)*(Q [J] +X[J]/K)*SQRT((R/K)↑2-(Q[J]+X[J]/K) ↑2)
                  +(1+(R/K)↑2/4)*(R/K)↑2*V [J]
                  +(Q[J] +X [J]/K)*SQRT(((R/K)↑2-(Q[J]+X[J]/K) ↑2)↑3)/6

52.     D=D+(C [J] -B [J] )*A [J] *7 End

53.     Print (FL)=D

54.     Carr (2) End

55.     End
```

In view of the approximations used in developing the solution, we should examine the limits and, if possible, the accuracy of the solution. The computer solution can be used only when the quantity

$$Q = \left(\frac{R}{K}\right)^2 - \left(\arctan \frac{W-X}{L} + \frac{X}{K}\right)^2 \geq 0 \qquad (A.18)$$

The value of R, the radius of the cylindrical tube, is fixed at 2.5 cm. A value of $K = 5$, i.e. 2.5 cm. of lead shielding was chosen as a basis for beginning calculations. A series of calculations showed that $0 < W \leq 1.5$, satisfied Equation A.18. Larger values of K are permitted, but smaller ones are not.

Equation A18 indicates that the minimum value of Q occurs when $x = W = \sqrt{KL-L^2}$, where $L = K - \sqrt{R^2 - W^2}$. For $W = 1.5$, $K = 5.0$, $R = 2.5$, the exact value of $\ln \frac{S_2}{S_1}$ is 0.27009. The approximate value is 0.14457. While this error is substantial, the extreme values are weighted relatively lightly in the integration, and the error in the less extreme cases, and hence in the integrated value will be proportionately much less.

Values of the integral were calculated for various values of W and K ranging from 0.7 to 1.5 and 5.0 to 10.0 respectively. For $R = 2.5$ and $K = 7.5$, a rough check was done on the computer solution. Eight values of $\ln \frac{S_2}{S_1}$ were calculated for representative values of ϕ and x. They ranged from 0.403 to 0.692 with an average of 0.635. If, as a very rough approximation, $\ln \frac{S_2}{S_1}$ is assumed constant

$$\int_{-\arctan \frac{W+X}{L}}^{\arctan \frac{W-X}{L}} \ln \frac{S_2}{S_1} \, d\phi \simeq 0.635 \left(\arctan \frac{W-X}{L} + \arctan \frac{W+X}{L}\right)$$

$$\simeq \frac{1.27\,w}{L}\left(1-\frac{1}{3}\frac{w^2}{L^2}-\frac{x^2}{L^2}\right) \qquad (A.19)$$

Then

$$\frac{1.27w}{L}\int_{-w}^{w}\left(1-\frac{1}{3}\frac{w^2}{L^2}-\frac{x^2}{L^2}\right)dx = \frac{2.54w^2}{L}\left(1-\frac{2w^2}{3L^2}\right) \qquad (A.20)$$

For $w = 1$, $L = 7.5 - \sqrt{6.25-1} \simeq 5.2$. The value of the integral is therefore 0.476. The value interpolated from computer calculations is 0.4[illegible]6.

There remains the problem of the slit thickness. The geometry of the arrangement is shown below.

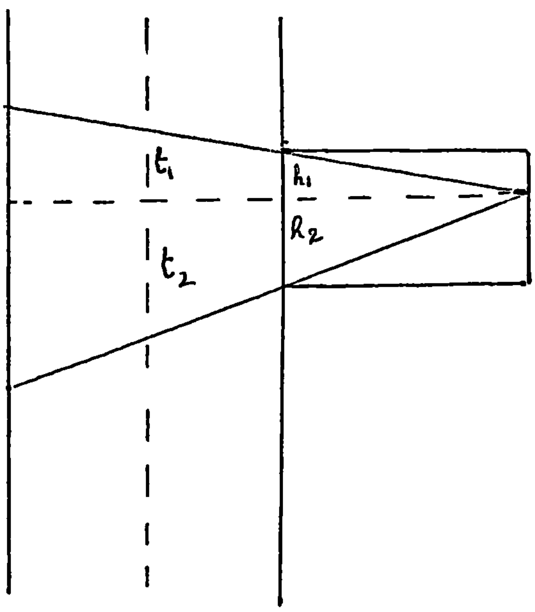

By similar triangles $\frac{t_1}{h_1} = \frac{K}{K-R}$ and $\frac{t_2}{h_2} = \frac{K}{K-R}$

Hence $t = \frac{K}{K-R}\,h$ where h = actual slit thickness.

This is only approximate because it does not take into account the effects of x and ϕ. It is now possible to tabulate values which have only to be multiplied by Sh^2 and the counting efficiency of the scintillation counter to give the radiation count which should be obtained.

TABLE 12

Values to be Multiplied by $c_{\gamma}SH^2$ to Obtain Counting Rate

		w (cm)							
		0.70	0.90	1.10	1.30	1.35	1.40	1.45	1.50
	5.0	0.1165	0.17773	0.2408	0.3022	0.3167	0.3305	0.3433	0.3560
	5.5				0.2252	0.2349	0.2464	0.2575	0.2682
	6.0	0.0610	0.0952	0.1326	0.1711	0.1805	0.1899	0.1991	0.2080
	6.5				0.1350	0.1428	0.1505	0.1582	0.1658
K(cm)	7.0	0.0373	0.0589	0.0833	0.1091	0.1156	0.1221	0.1285	0.1343
	7.5				0.0899	0.0954	0.1009	0.1064	0.1118
	8.0	0.0251	0.0399	0.0570	0.0754				
	9.0	0.0180	0.0288	0.0414	0.0551				
	10.0	0.0135	0.0218	0.0314	0.0420				

Theoretical Counting Efficiency

When radiation from a point source impinges on a crystal, the counting rate depends upon both the solid angle and the counting characteristics of the crystal. As these are interrelated, they are normally combined in an absolute counting efficiency[35]. In the present case, however, the narrow slit permits radiation to fall on only the centre portion of the crystal and it is the view factor rather than the solid angle which must be considered. Hence, the counting characteristics of the crystal must be determined by taking account of the effect of solid angle on the absolute counting efficiency.

A further complication is that not all the Compton-scattered photons are counted. Also, in the case of Pr^{142}, only part of the disintegrations result in gamma radiation. Thus

$$c_s = \left(\frac{St_1}{4\pi} \cdot D\right)\left(\frac{\varepsilon_\gamma}{\varepsilon_g}\right)(f_\gamma)(f_c) \tag{A.21}$$

where

c_s = counting rate for photons coming through the slit (i.e. without penetrating any lead)

D = view factor

ε_γ = total absolute counting efficiency

ε_g = solid angle

f_γ = fraction of disintegrations which produce gamma radiation

f_c = fraction of total absolute efficiency obtained when lower energy photons are cut off.

If the geometry of the experimental apparatus corresponded exactly to that for which the calculations were made, the view factor, D, would be the result obtained when the right hand side of Equation A.17 is integrated with respect to x between the limits -w and w (page 70). Then the result would be given by the computer programme (statement 53, page 72).

For the actual apparatus, the view factor is not given exactly by the programme, but a good estimate can be made. The value of K (page 68) is 9. In the limit, doubling the area of exposed detector doubles the view factor for large values of K. This gives the slope of the view factor vs w curve at w = 2.5 cm. When calculated values of the view factor are plotted against w, a smooth curve gives a value of about 1.18 for w = 2.5 cm. If, with the actual slit of w = 0.95 cm., all the exposed area of the detector "saw" all parts of the slurry, the view factor, D, would be 0.41. In actual fact, it will be less than this but more than the value of 0.29 corresponding to the theoretical geometry for w = 0.95 cm. As these values are not too far apart, the intermediate value of D = 0.35 may be chosen.

For a thin cylindrical 5 mc source,

$$\frac{St}{4\pi} = \frac{(5\times10^{-3})(3.7\times10^{10})}{\pi(2.45)^2(4\pi)} = 7.80 \times 10^5$$

The thickness of the slit, h, is 0.318 cm. The factor ($\frac{St}{4\pi}$ h D) in Equation A.21 is therefore $(7.80 \times 10^5)(0.318)(0.35) = 8.69 \times 10^4$.

The area of one end of the crystal is $\pi(2.254)^2/4 = 6.45\ \pi$ sq.cm. The area of a spherical surface of radius $4\pi r^2$. Hence the solid angle ε_g is very nearly $1.612/r^2$. If the efficiency of a scintillation counter varied only with the solid angle, $\varepsilon_\gamma/\varepsilon_g$ would be invariant and hence $\varepsilon_\gamma r^2$ would be almost constant. Values of ε_γ for various values of r were obtained from Heath's report[35] and $\varepsilon_\gamma r^2$ was plotted against r. For values of r from 2 to 10 inclusive, a straight line was obtained on a semilog plot. On this basis, $\varepsilon_\gamma r^2$ for r = 9 is 0.613 and $\varepsilon_\gamma/\varepsilon_g$ = 0.613/1.612 = 0.380 for r = 9 cm. As the gamma rays hit very close to the centre of the detector, the ratio may be considerably greater[35] than this average value. The upper limit is, of course, 1.00. A value of $\varepsilon_\gamma/\varepsilon_g = 0.76$ was chosen.

The factor f_c was evaluated by assuming that the peak constitutes about 30% of the total count[35]. On the basis of a cut-off at 400 and a peak at 505 pulse height units,

$$f_c = \frac{1 + \left(\frac{0.7}{0.3}\right)\left(\frac{105}{505}\right)}{1 + \frac{0.7}{0.3}} = 0.45$$

As only 4% of the disintegrations for Pr^{142} result in gamma radiation[36], $f_\gamma = 0.04$.

Substitution of all these factors into Equation A.21 gives

$$c_g = (8.69 \times 10^4)(0.76)(0.04)(0.45) = 71{,}500 \text{ counts/min.}$$

It is not possible to calculate exactly the additional radiation which passes through various thicknesses of lead to reach the crystal or is scattered back into the slit. Obviously this will be greater near the slit. A very approximate estimate can be obtained. The total absolute efficiency of the detector is 0.613/81 = 0.757×10^{-2}. A thickness of lead shielding of 4.6 cm reduces the radiation[34] by a factor of $e^{-0.57(4.6)} = 0.0725$. The number of gamma rays emitted is (5×10^{-3}) (3.7×10^{10}) $(4 \times 10^{-2}) = 7.4 \times 10^6$ gammas/sec. Using the same set as before, we obtain (7.4×10^6) (0.757×10^{-2}) (0.45) (0.725×10^{-1}) = 1.83×10^3 counts/sec = 109,800 counts/min. This value is probably low because of the large amount of Compton-scattered photons which will be absorbed and for which the counting efficiency is slightly higher.

The total is therefore about 200,000 counts/min. Because of the large number of approximations and estimates, this cannot be more than a very rough value.

Penetration of Lead Shielding

As Pr^{142} has a "hard" gamma (1.57 Mev), radiation from the column will pass through the lead shielding and be counted. For the experimental set-up postulated in the previous section, the calculation of "extraneous" radiation would be very complex. A rough estimate can be obtained by a comparison with the gamma-ray intensity from a shielded infinite line source(34).

If s' is the source strength per cm of length, u is the absorption coefficient (0.57 for Pr^{142} in lead), and K and R have their previous meanings.

$$I = \frac{s' \operatorname{seci} u(K-R)}{2\pi(K-R)}$$

where seci(x) is a function defined $= \int_0^{\pi/2} e^{-x\sec\theta}\, d\theta$. Using values of seci(x) from Henderson and Whittier(34), the factor $\frac{\operatorname{seci}(uy)}{y}$ was calculated for a number of thicknesses of shielding.

K-R	u(K-R)	seci u(K-R)	$\frac{\operatorname{seci} u(K-R)}{(K-R)}$
2.5	1.43	0.17	0.068
3.5	2.00	0.090	0.026
4.5	2.57	0.048	0.011
5.5	3.14	0.025	0.0045
6.5	3.71	0.013	0.0020
7.5	4.28	0.0068	0.00091

Although the "extraneous" radiation falls off rapidly with increasing thickness of shielding, the "desired" radiation does also. It is possible to make a rough estimate of the ratio of extraneous to desired radiation. As in the previous section, we assume that the efficiency of the detector is twice as great for radiation hitting its center, and that the radiation which does not pass through lead constitutes 35% of the total counted from a cylindrical element directly in front of the slit.

With the actual experimental apparatus, the thickness of absorbing lead was 4.6 cm. while the perpendicular distance from the "line source" was 9.1 cm. Thus

$$I_{ext} = \frac{s' \quad (0.57)(4.6)}{2\pi\ (9.1)} = \frac{s'(0.044)}{18.2\pi} = \frac{2.42x10^{-3}s'}{\pi}$$

The "line" source strength, s', is related to the volume source strength, s, by $s' = \pi R^2 s$ so that

$$I_{ext} = 2.42x10^{-3}\ (6.25)s = 1.51x10^{-2}s$$

The extraneous radiation has the advantage of a larger available detector area. The projected area perpendicular to the radiation varies from 20.3 sq.cm for the circular end, to 23.7 for the most elongated ellipse back to 25.8 for square "seen" from infinity. As the near values are weighted most heavily; we choose a value of 23 sq.cm.

By geometry, the detector sees a slice of slurry 0.618 cm thick when the slit thickness is 0.318 cm. From the previous section the partial view factor is 0.35. The ratio of counts is therefore

$$\frac{\frac{s(0.618)}{4\pi}\ (0.35)(0.318)(2/0.35)}{1.51x10^{-2}s\ (23)} = \frac{0.0313}{0.347}$$

This is approximately the ratio of counts from a cylindrical section 0.618 cm high to the count which would be obtained from the whole column if the slit were absent. About 35% of the numerator can be attributed to the presence of the slit. Therefore the ratio of counts from the cylindri-

cal section to the total count is approximately $\frac{0.0313}{0.347+0.011} = 8.7\%$.
This means that the counts received from the slurry very close to the slit will be only a small fraction of the total count.

NOMENCLATURE

B = constant

c = solids concentration, g/cc.

d = diameter of particles

D = degree of dilution, dimensionless (g.fluid/g.solid)

g = gravitational constant, cm/min^2

k = constant, dimensions vary with equation

n = dimensionless constant

S = solids flux

t = time, minutes

u = settling rate, cm/min

u_o = Stokes' velocity of a particle or floc, cm/min

z = height measured from bottom of settling column, cm

Greek Letters

α = constant, min/cm

β = constant, cm^{-1}

β_e = correction factor for Stokes' velocity

δ = propagation velocity of a concentration or concentration discontinuity cm/min

ε = voidage, dimensionless

μ = viscosity, g/min.cm

ρ = density, g/cc

ϕ = volume ratio of floc to solids in the floc, dimensionless

REFERENCES

1. Coe, H.S. and Clevenger, G.H., Trans Am. Inst. Mining Engrs., 55, 356(1916)
2. Mishler, R.T., Eng. Mining J., 94, 643 (1912)
3. Doane, W.H. Trans.Am.Electrochem.Soc., 37, 71 (1920)
4. Deerr, N., Intern.Sugar J., 22, 618 (1920)
5. Robinson, C.S., Ind.Eng.Chem., 18, 869 (1926)
6. Egolf, C.B., and McCabe, W.L., Trans.Amer.Inst.Chem.Engrs., 33, 620 (1937)
7. Ward, H.T. and Kammermeyer, K., Ind.Eng.Chem., 32, 622 (1940)
8. Work, L.T., and Kohler, A.S., Ind.Eng.Chem, 32, 1329 (1940)
9. Commings, E.W., Ind. Eng.Chem., 32, 663 (1940)
10. Kammermeyer, K., Ind. Eng.Chem., 33, 1484 (1941)
11. Roberts, E.J., Mining Eng., 1, 61 (1949)
12. Richardson, J.F., and Zaki, W.N., Trans.Inst.Chem.Engrs., 32, 35(1954)
13. Lewis, W.K., Gilliland, E.R., and Bauer, W.C., Ind.Eng.,Chem., 41 1104 (1949)
14. Richardson, J.F., and Zaki, W.N., Chem.Eng.Sci., 3, 65 (1954)
15. Andreo, U.T., C.A. 54, 21883e
16. Gasparayan, A.M. and Zaminyan, A.A., C.A. 54, 23487i
17. Michaels, A.S. and Bolger, J.C., Ind.Eng.Chem. Fundamentals 1, 24 (1962)
18. Steinour, H.H., Ind.Eng.Chem., 36, 618-24; 840-7; 901-907 (1944)
19. Bond, A.W., Proc.Am.Soc.Civil.Engrs., 86, No. SA_3, 57 (1960)
20. Kynch, G.J., Trans.Faraday Soc., 48, 166 (1952)
21. Yoshika, N., Hotta, Y. and Tanaka, S., Chem.Eng. (Japan), 19, 616 (1955)
22. Smelli, R.H. and Lamer, V.K., J.Colloid.Sci., 11, 704 (1956)

23. Shannon, P.T., Stroupe, E.P. and Tory, E.M., Ind.Eng.Chem. Fundamentals 2, 203 (1963)

24. Shannon, P.T., Stroupe, E.P., and Tory, E.M., Am.Chem.Soc.Meeting, September 10, 1963.

25. Shannon, P.T., DeHaas, R.D. and Tory, E.M., Ind.Eng.Chem. Chem.Eng. Symposium, November 14-15, 1963.

26. Tory, E.M., Ph.D. Thesis, Purdue University (1961)

27. Hassett, N.J. Ind. Chem., 34, 489 (1958)

28. Wallis, G.B., 3rd. Congress of European Federation of Chemical Engineers (London) June 1962.

29. Boyd, A.W., and Witton, J.L., Can.J. of Chem.Eng., 36, 277 (1958)

30. Reich, I. and Vold, R.D., J.Phys. Chem., 63, 1497 (1957)

31. Gaudin, A.M., Fuerstenau, M.C. and Mitchell, S.R., Mining Eng., 11, 613 (1959)

32. Richarson, J.F. and Shabi, F.A., Trans. Inst. Chem.Engrs., 38, 33 (1960)

33. Summer, D.B., Private Communication January 23, 1963.

34. Henderson, W.J. and Whitter, A.C., Handbook of Shielding and Heat Production Calcul tions for the N.R.U. Reactor, AECL No.403,

35. Heath, R.L., Scintillation Spectrometry Gamma-Ray Spectrum Catalogue AEC Research and Development Report.

36. Strominger, D., Hollander, J.M. and Seaborg, G.T., Rev.Mod.Phy, 30, 585 (1958)